Journal for ImmunoTherapy of Cancer

PP4 inhibition sensitizes ovarian cancer to NK cell-mediated cytotoxicity via STAT1 activation and inflammatory signaling

Remya Raja,[1] Christopher Wu,[1] Esen Yonca Bassoy,[1] Thomas E Rubino Jr,[1] Emma C Utagawa,[1] Paul M Magtibay,[2] Kristina A Butler,[2,3] Marion Curtis [1,3,4]

To cite: Raja R, Wu C, Bassoy EY, *et al*. PP4 inhibition sensitizes ovarian cancer to NK cell-mediated cytotoxicity via STAT1 activation and inflammatory signaling. *Journal for ImmunoTherapy of Cancer* 2022;**10**:e005026. doi:10.1136/jitc-2022-005026

► Additional supplemental material is published online only. To view, please visit the journal online (http://dx.doi.org/10.1136/jitc-2022-005026).

Accepted 28 November 2022

[1]Department of Immunology, Mayo Clinic Scottsdale, Scottsdale, Arizona, USA
[2]Department of Gynecology, Mayo Clinic, Scottsdale, Arizona, USA
[3]College of Medicine and Science, Mayo Clinic, Scottsdale, Arizona, USA
[4]Department of Cancer Biology, Mayo Clinic Arizona, Scottsdale, AZ, USA

Correspondence to
Dr Marion Curtis;
curtis.marion@mayo.edu

ABSTRACT

Background Increased infiltration of T cells into ovarian tumors has been repeatedly shown to be predictive of enhanced patient survival. However, despite the evidence of an active immune response in ovarian cancer (OC), the frequency of responses to immune checkpoint blockade (ICB) therapy in OC is much lower than other cancer types. Recent studies have highlighted that deficiencies in the DNA damage response (DDR) can drive increased genomic instability and tumor immunogenicity, which leads to enhanced responses to ICB. Protein phosphatase 4 (PP4) is a critical regulator of the DDR; however, its potential role in antitumor immunity is currently unknown.

Results Our results show that the PP4 inhibitor, fostriecin, combined with carboplatin leads to increased carboplatin sensitivity, DNA damage, and micronuclei formation. Using multiple OC cell lines, we show that PP4 inhibition or *PPP4C* knockdown combined with carboplatin triggers inflammatory signaling via Nuclear factor kappa B (NF-κB) and signal transducer and activator of transcription 1 (STAT1) activation. This resulted in increased expression of the pro-inflammatory cytokines and chemokines: *CCL5*, *CXCL10*, and *IL-6*. In addition, *IFNB1* expression was increased suggesting activation of the type I interferon response. Conditioned media from OC cells treated with the combination of PP4 inhibitor and carboplatin significantly increased migration of both CD8 T cell and natural killer (NK) cells over carboplatin treatment alone. Knockdown of stimulator of interferon genes (STING) in OC cells significantly abrogated the increase in CD8 T-cell migration induced by PP4 inhibition. Co-culture of NK-92 cells and OC cells with *PPP4C* or *PPP4R3B* knockdown resulted in strong induction of NK cell interferon-γ, increased degranulation, and increased NK cell-mediated cytotoxicity against OC cells. Stable knockdown of PP4C in a syngeneic, immunocompetent mouse model of OC resulted in significantly reduced tumor growth *in vivo*. Tumors with PP4C knockdown had increased infiltration of NK cells, NK T cells, and $CD4^+$ T cells. Addition of low dose carboplatin treatment led to increased $CD8^+$ T-cell infiltration in PP4C knockdown tumors as compared with the untreated PP4C knockdown tumors.

Conclusions Our work has identified a role for PP4 inhibition in promoting inflammatory signaling and enhanced immune cell effector function. These findings support the further investigation of PP4 inhibitors to enhance chemo-immunotherapy for OC treatment.

WHAT IS ALREADY KNOWN ON THIS TOPIC

⇒ Deficiencies in the DNA damage response (DDR) have been shown to promote an immune response against multiple cancers, including ovarian cancer (OC), and to synergize with immune checkpoint blockade (ICB). Combining DDR inhibitors with ICB represents an attractive therapeutic strategy.

WHAT THIS STUDY ADDS

⇒ Using *in vitro* cell-based assays and *in vivo* mouse models we identified a role for protein phosphatase 4 (PP4) in augmenting inflammatory signaling and immune cell infiltration.

HOW THIS STUDY MIGHT AFFECT RESEARCH, PRACTICE OR POLICY

⇒ Our work indicates that targeting PP4 in combination with platinum-based therapy represents a promising strategy to improve the antitumor immune response in OC.

BACKGROUND

High-grade serous ovarian cancer (OC) remains one of the most frequent causes for cancer-related death among women in the USA.[1] Frontline treatment strategies for patients with OC include cytoreductive surgery combined with taxane or platinum-based chemotherapy. However, the emergence of platinum resistance is frequent, and the overall 5-year survival rate remains near 30%.[2] Immune checkpoint blockade (ICB) has been shown to induce durable responses in multiple cancer types. However, the benefit of ICB remains largely restricted to a minority of patients.[3] Multiple reports have confirmed that increased tumor-infiltrating T cells is correlated with improved clinical outcomes in OC.[4 5] Despite these findings, ICB has produced minimal clinical benefit for patients with OC and as a result there are no Food and Drug Administration approved immunotherapies for OC.[6] These results underscore the

need for the development of new rationally designed therapeutic approaches to improve outcomes for patients with OC.

Recent studies have shown that defects in DNA damage response (DDR) pathways can lead to increased genomic instability and tumor immunogenicity, which leads to enhanced responses to checkpoint inhibitor therapy.[7 8] Homologous recombination (HR) defects are prevalent in OC. Poly (ADP-ribose) polymerase (PARP) inhibitors are now approved for maintenance therapy in recurrent, chemosensitive OC irrespective of BRCA1/2 mutation status.[9] Several studies now indicate that PARP inhibitors can increase the response rate to ICB.[10 11] This suggests that modulation of the DDR in OC may be one-way to increase response to ICB and the identification of additional molecular targets is of translational interest.

Protein phosphatase 4 (PP4) is a multisubunit Ser/Thr phosphatase complex that is involved in diverse cellular pathways including DDR, cell cycle progression, and apoptosis.[12] PP4 plays a central role in the response to DNA damage as it directly dephosphorylates many proteins that play crucial roles in the DDR, including γH2AX, Kap-1/TRIM28, RPA2, and 53BP1.[13–16] Dephosphorylation of these critical substrates is necessary for resolution of DDR. We previously discovered that the cancer/testis antigen, CT45, directly binds to the PP4 complex and functions as an endogenous inhibitor of PP4 activity leading to enhanced platinum sensitivity and DNA damage.[17] In addition, patients whose tumors have increased levels of the catalytic subunit, PP4C, were found to have reduced overall survival.[17] However, the role of PP4 in antitumor immunity is currently not known. In this study, we used a combination of the PP4 inhibitor, fostriecin, and transient or stable PP4 knockdown to interrogate the role of PP4 in chemosensitivity and in immune effector function in OC.

METHODS

Cell lines

High-grade serous OC cell lines NIH-OVCAR3, OVCAR4 and OVCAR8 were obtained from the NCI-Frederick Cancer DCTD Tumor/Cell Line repository and ID8 was purchased from Millipore. The OC cell lines, NIH-OVCAR3, OVCAR4, and OVCAR8 were cultured in RPMI with 10% fetal bovine serum (FBS) and 1% penicillin/streptomycin. The mouse OC cell line, ID8, was cultured in Dulbecco's modified eagle's media (DMEM) with 4% FBS, 1X Insulin-Transferrin-Selenite and 1% penicillin/streptomycin. The natural killer (NK)-92 cell line was a kind gift from Abhinav Acharya, Arizona State University, USA. The OVCAR8-DR-GFP cell line was a kind gift from Dr Larry Karnitz, Mayo Clinic, Rochester, USA. The cells were grown in complete RPMI media with 30 µg/mL puromycin. All cell lines were tested for mycoplasma and authenticated using a commercial service (CellCheck, IDEXX Bioresearch).

ID8 p53 CRISPR/Cas9 knockout cell generation

A p53 knockout clone was generated from ID8 (ID8-p53KO) using CRISPR/Cas9. Three CRISPR RNA (crRNA) targeting the DNA binding domain of p53 were selected as described previously.[18] Predesigned guides with the highest on-target and cutting efficiency scores were purchased from Integrated DNA Technologies in their proprietary Alt-R format (online supplemental table 1). crRNA-trans-activating CRISPR RNA (tracrRNA) duplexes were prepared by annealing equimolar concentrations of AltR crRNA with Alt-tracrRNA-ATTO 550 at 95°C for 5 min in a thermocycler and allowing it to slowly cool to room temperature. In a PCR strip, three crRNA-tracrRNA duplexes were mixed with recombinant Cas9 V3 protein (#1081058, Integrated DNA Technologies) and incubated for 20 min. ID8 cells were electroporated (BTX ECM 830, Harvard Apparatus) with ribonucleoprotein complex and electroporation enhancer (#1075915, IDT). The gene edits in single clones were verified by Sanger sequencing and p53 protein knockout was confirmed using western blot.

Transfection and stable cell line generation

Human and mouse siGENOME SMARTpool *PPP4C* siRNA, human *PPP4R3B,* ON-TARGETplus SMARTpool human *STING1* siRNA, and non-targeting control pool #2 were purchased from Horizon Discovery Biosciences. Transfection with siRNAs were performed with Lipofectamine 3000 as per manufacturer's protocol. For stable knockdown of PP4C, ID8-p53KO cells were transfected with either lentiviral pLKO.1 (Addgene) or mouse *PPP4C* shRNA-pLKO.1 puro (Millipore, Sigma) followed by puromycin selection.

Bioinformatics analysis

Genome profiling of PP4 complex members, namely *PPP4C*, *PPP4R3A*, *PPP4R3B* and *PPP4R2*, across different cancer types was performed using the pan-cancer The Cancer Genome Atlas (TCGA) data available at cBioPortal (https://www.cbioportal.org/).[19] The OncoPrint for PP4 subunits in OC (TCGA, pan-cancer atlas) was also created using the relevant module at cBioPortal. RNA sequencing (RNA-seq) expression values (transcripts per million; TPM) were obtained for *PPP4C, PPP4R3A, PPP4R3B* and *PPP4R2* from OC (TCGA) and normal ovaries/fallopian tubes (GTEx) using the UCSC Cancer Browser (https://xena.ucsc.edu/welcome-to-ucsc-xena/).[20] From the DepMap database (https://depmap.org/portal/), RNA level expression values and proteomic scores for PP4C were obtained for relevant OC cells and plotted.[21] The Tumor IMmune Estimation Resource (TIMER) V.2.0 (https://timer.cistrome.org/) gene module was used to analyze the correlation between the tumor-specific gene expression of PP4 subunits and immune cell infiltration, particularly for NK and NK T-cell populations. The purity corrected OC data set (n=303) was analyzed using benchmarked CIBERSORT and xCell deconvolution tools.[22 23]

Incucyte live-cell imaging and cell viability analysis

For cell viability analysis with fostriecin, the ID8 p53-WT cell line was seeded in a 96-well plate. At 24 hours, cells were pretreated with fostriecin (1 nM), the control cells were left untreated. After 24 hours, control and fostriecin pretreated cells were treated with varying concentrations of carboplatin (1µM- 1 mM). For live cell imaging and cell proliferation, Incucyte images were taken every 4 hours and cell confluence was recorded. For siRNA experiments, both ID8-p53WT and p53KO cells were transfected with *PPP4C* siRNA followed by carboplatin treatment for 96 hours. Cell viability was measured by CellTitre 96 AQueous Non-Radioactive Cell Proliferation Assay (#G5421, Promega) as per manufacturer's instructions.

Clonogenic survival assay

Cells were treated with different carboplatin concentrations (as indicated in the figure legends) for 96 hours. A total of 2000 cells per 6-well were then plated for 7 days in drug-free medium. Colonies were fixed with 1% formaldehyde for 10 min at room temperature and stained with 40% methanol and 0.05% crystal violet for 20 min. The colonies were counted using the Colony Area ImageJ plugin and plotted as percent survival of control.[24]

Immunoblotting

Western blot was performed as described previously.[17] OC cells were pretreated with fostriecin (1 nM) on day 1, post seeding. The cells were treated with carboplatin at indicated doses±fostriecin (1 nM) on day 2. On day 5, cells were collected in radioimmunoprecipitation assay (RIPA) buffer and lysates prepared for SDS-PAGE and immunoblot analysis. The list of antibodies used in the study is listed in online supplemental table 2.

Phosphatase activity assay

Cellular PP4 activity in OC cells was performed as described previously with minor modifications.[17] Immunoprecipitation was carried out from lysates (1 mg) using anti-PPP4C antibody or Control IgG, followed by incubation with Protein-A Agarose beads (#22811, Thermo Scientific) overnight at 4°C. The washed beads were resuspended in 100 µL assay buffer (30 mM of N-2-hydroxyethylpiperazine-N-2-ethane sulfonic acid (HEPES), 0.1 mg/mL of bovine serum albumin, 0.1 mM of MnCl2, 1 mM of sodium ascorbate, 1 mM of DTT, 0.01% Triton X-100) ± fostriecin (1 nM) and incubated at room temperature for 30 min. PP4 activity was assayed by incubating the washed beads with 100 µM DiFMUP substrate (#D6567, Invitrogen) and fluorescence measured at 450 nM after 60 min using FlexStation 3 (Molecular Devices). PP4 activity is shown as a percentage of untreated control.

Immunofluorescence and micronuclei analysis

OVCAR3, OVCAR4, OVCAR8 and ID8-p53KO cells were seeded in a 96-well plate and treated±fostriecin (1 nM), followed by carboplatin at indicated doses: OVCAR3 and 4 (1µM), OVCAR8 (2.5 µM) and ID8-p53KO (10 µM). At 96 hours, cells were washed with 1× phosphate buffered saline (PBS), followed by fixation for 10 min at room temperature with 4% paraformaldehyde. The cells were stained with Hoechst 33 342 (#H3570, Invitrogen) for 10 min and micronuclei were imaged using ImageXpress (Molecular Devices). A minimum of 45–50 sites were imaged per conditions and represented as violin plots. Immunofluorescence analysis with γ-H2AX (S139), (#MA1-2022, Thermo Fisher Scientific) and FANCD2 (#ab108928, Abcam) in OVCAR3 was performed as described previously.[17]

Cellular thermal shift assay

The assay was performed as described previously with minor modifications.[25 26] Briefly, OVCAR4 and OVCAR3 cells were collected in PBS with 1 mM sodium ascorbate, incubated±fostriecin (1 nM) for 30 min and subjected to increasing temperatures. Cells were lysed and immunoblotting was done for PP4C. The densitometry on immunoblots was performed with ImageJ (National Institutes of Health), and relative band intensities were quantified as percentage of non-denatured protein.

qRT-PCR

The OC cells were treated with fostriecin (1 nM) on day 1, followed by carboplatin treatment at indicated doses±fostriecin on day 2. The cells were harvested on day 5 post-carboplatin treatment for quantitative PCR. For siRNA experiments, cells were transfected with *PPP4C* or control siRNA on day 1, followed by carboplatin treatment on day 2. The cells were harvested on day 5. The primers used for quantitative reverse transcription PCRqRT-PCR are listed in online supplemental table 3.

Cytokine array

OVCAR3 cells were transfected with control or *PPP4C* siRNA, followed by carboplatin treatment (1 µM). At 72 hours, post-carboplatin treatment, culture media was replaced with basal RPMI-1640 with 0.2% BSA. Conditioned media was collected after 48 hours. The Human Cytokine Array, C5 (Ray Bio; AAH-CYT-5–4) was used to analyze 80 different cytokines. Expression levels were analyzed using Protein Array Analyzer macro (http://rsb.info.nih.gov/ij/macros/toolsets/Protein Array Analyzer.txt with ImageJ software.[26]

DR-GFP HR assay

HR assays were performed using OVCAR8-DR-GFP cells. The experiments were performed as described previously with minor modifications.[27] For siRNA experiments, the cells were transfected twice. On day 1, they were transfected with *PPP4C* or control siRNA only. On day 2, cells were transfected with 4 µg pCßASceI plasmid (encoding I-SceI), empty vector (pcDNA3.1) and mCherry (pCDNA3.1). GFP and mCherry fluorescence were assessed by flow cytometry on day 5. For inhibitor experiments, OVCAR8-DR GFP cells were transfected with pCßASceI, empty vector (pcDNA3.1) and mCherry (pCDNA3.1) plasmids on day 1, followed by B-02 (RAD51

inhibitor) or fostriecin at indicated doses. HR efficiency was calculated as GFP and mCherry positive cells/mCherry positive cells.

CD8 T cell and NK cell migration

ID8-p53KO or OVCAR3 cells were treated with fostriecin (1 nM) on day 1, followed by carboplatin (10 µM) ± fostriecin (1 nM) on day 2. The media was changed to basal RPMI-1640+0.5% BSA after 72 hours of carboplatin treatment. The conditioned media was collected after 48 hours. OT-I splenocytes were isolated and stimulated with chicken ovalbumin (OVA) peptide (SIINFEKL) in presence of interleukin (IL)-2. On day 3 following OVA stimulation, CD8 T cells were enriched using mouse CD8a T-cell positive selection kit (#18953, STEMCELL) according to the manufacturer's instructions. Mouse CD8 T or NK-92 (1e5) cells were placed in basal media in the upper chamber of 5 micron filters, conditioned media corresponding to various treatments from ID8 and OVCAR3 were placed in the lower chamber, respectively.[28 29] The migrated cells were collected at 4 hours and quantified with CellTitre-Glo 2.0 reagent (#G9241, Promega). For inhibitor experiments, CD8 T cells or NK-92 cells were incubated with either Stattic (2 µM) or trametinib (7.5 µM) or NSC23766 (10 µM) for 15 min at 37°C, prior to adding to the upper chamber.

Intracellular cytokine staining

OT-I splenocytes were stimulated with OVA (30 ng/mL) ± fostriecin at 1 and 10 nM. At 72 hours, cells were restimulated with OVA peptide in presence of GolgiPlug and incubated for 4 hours at 37°C in a 5% CO2 incubator. The cells were surface markers (anti- mouse-CD3, CD8, live/dead stain). Cells were fixed, permeabilized and stained for cytokines using an anti-interferon (IFN)-γ and tumor necrosis factor (TNF)-α antibody. For cell co-culture experiments, OVCAR8 cells were treated with fostriecin or transfected with either *PPP4C* or control or *PPP4R3B* siRNA, followed by carboplatin treatment (2.5 µM). On day 5, cells were trypsinized and seeded on to a flat bottom 12-well plate. After 6 hours, NK-92 cells were added in a 1:1 (tumor:NK cell) ratio. At the end of 14 hours co-culture, NK-92 cells were collected and restimulated with cell stimulation cocktail (#TNB-4975-UL100, Tonbo Biosciences) for 4 hours and transferred to Laminar Wash 96-well plate (Curiox Biosystems, Seoul, South Korea) for intracellular staining. Cells were washed by laminar flow (8–10 cycles) using the Curiox Laminar Wash System HT1000. All antibodies used in flow cytometry are provided in online supplemental table 4. Flow data analysis was performed with FlowJo (V.10.8.0)

CD107a mobilization and NK cell cytotoxicity assay

OVCAR8 cells were transfected with respective siRNAs and treated with carboplatin at 2.5 µM. On day 5, cells were washed, trypsinized and mixed with NK-92 in 1:1 ratio (target:effector) in a U-bottom 96-well plate. CD107a antibody was added at the beginning of the experiment and cells were co-cultured for 3 hours in the presence of GolgiPlug and Monensin. At the end of 3 hours, cells were stained with cell surface markers and analyzed by flow cytometry. For cytotoxicity assays, OVCAR8 cells were treated as described previously and on day 5, cells were mixed with NK-92 cells in 1:1 ratio (target:effector) in a U-bottom 96-well plate. At the end of 3 hours incubation, cells were stained with anti-annexin V and propidium iodide.

In vivo experiments

Female C57BL/6 mice (8 weeks) were injected with 1 million ID8-p53KO-control-Luc and ID8-p53KO-ppp4c sh2-luc cells intraperitoneally. Mice were housed under standard living conditions with routine light/dark cycle and treatment was performed during the light cycle. After 7 days, carboplatin was administered intraperitoneally two times a week at 5 mg/kg. The control group was treated with sterile PBS. Tumor growth was monitored weekly by luminescence imaging and the health status of the mice was monitored daily. On days 28–30 post implantation, tumors were harvested, and weights were recorded. Ascites, peritoneal lymph nodes, and spleens were also collected at the time of necropsy for immune cell phenotyping.

Tissue processing and *ex vivo* immune cell analysis

The tumors and lymph nodes collected from mice were mechanically dissociated. Lymph nodes were incubated in 2 mL tissue dissociation media (RPMI-1640 media; Fisher Healthcare; MT10040CV) supplemented with 0.5% BSA (Sigma-Aldrich; A1470), 0.75 mg/mL collagenase (Type II; Thermo Scientific; 17,101–015), 30 µg/mL DNase I (Sigma-Aldrich; 10104159001) at 180 rpm (shaking) 37°C for 20 min. Tumor tissue dissociation was done with the gentleMACS Octo dissociator with heaters (Miltenyi Biotec) using 2.5 mL tissue dissociation media. Cell suspensions were filtered through 70 micron nylon cell strainer (Fisher Scientific; 22-363-548). For *ex vivo* restimulation, cells were treated with Cell Stimulation Cocktail (Tonbo Biosciences, TNB-4975-UL400) for 4 hours, followed by cell surface and intracellular staining. Absolute counting beads (Thermo Scientific, C36950) were included to obtain total cell counts in the samples. All antibodies used for flow cytometry are provided in online supplemental table 4.

Statistical analysis

All statistical analyses were performed with GraphPad Prism (GraphPad) software V.9. For experiments with one comparison an un-paired, two-tailed t-test was used. The mean and the SEM or SD are reported for all graphs. For experiments with more than one comparison, One-way analysis of variance (ANOVA) with Tukey's multiple comparisons post-test was used. Before applying ANOVA, we first tested whether the variation was similar among the groups using the Bartlett's test. Differences were considered significant if $p<0.05$. No blinding or

randomization was done during data acquisition or assessment of outcome and sample sizes were determined based on previous experience with the individual experiment.

RESULTS

Overexpression of PP4 subunits in OC

The PP4 holoenzyme consists of the catalytic subunit (PP4C) and multiple different regulatory subunits: PP4R1, PP4R2, PPP4R3β and PPP4R3α. The catalytic subunit forms distinct complexes with different regulatory subunits that have been shown to influence both PP4 enzyme activity and substrate selectivity.[14] We previously identified CT45 as an endogenous inhibitor of PP4 complex that physically interacts with the PP4C-PPP4R2-PPP4R3α/β complex leading to enhanced carboplatin sensitivity in OC.[17] To better understand the role of PP4 in cancer we investigated the genome level alterations of *PPP4C*, *PPP4R3A*, *PPP4R3B* and *PPP4R2* subunits using the pan-cancer TCGA data in cBioPortal (n=10953). We found that the PP4 subunit genes are predominantly amplified in roughly 6% of OC tumors (figure 1A, online supplemental figure 1A). Similar to OC, invasive breast carcinoma, bladder urothelial carcinoma, and seminoma also showed significant amplification of PP4 subunit genes (figure 1A). In addition, we observed significant concordance between messenger RNA (mRNA) levels and amplification of *PPP4C* in the pan-cancer TCGA data (figure 1B) as well as for the

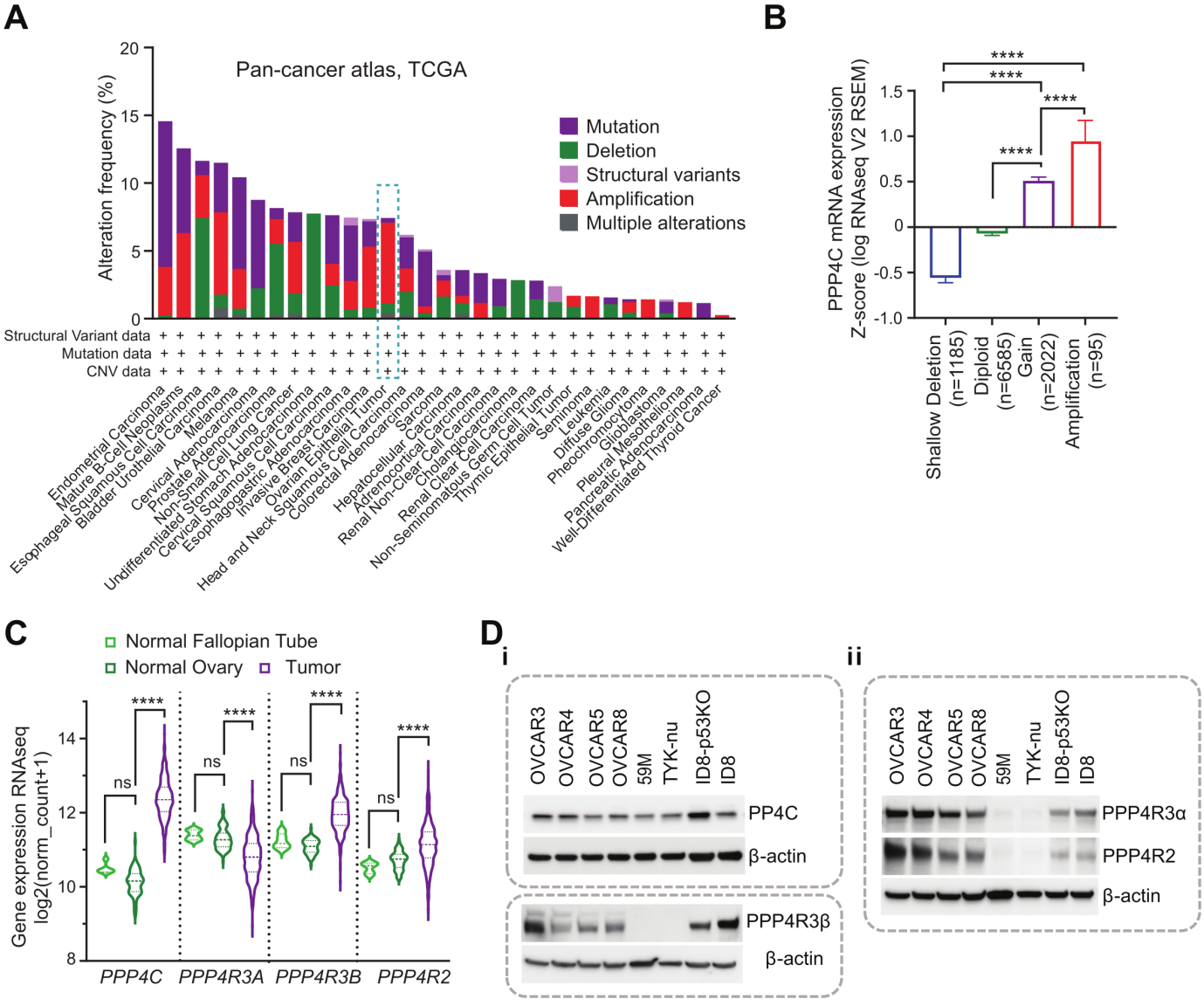

Figure 1 PP4 subunits are amplified in ovarian cancer. (A) Genomic profiling of PP4 across human cancers using TCGA data from cBioPortal. (B) *PPP4C* mRNA expression versus copy number from pan-cancer TCGA data is plotted as a bar graph, ****p<0.0001. (C) Comparison between transcript level expression of PP4 subunits (transcripts per million) compared between TCGA ovarian tumor cohort (n=418) and normal ovary (n=88) and fallopian tube (n=5) (GTEx); ns, not significant, ****p<0.0001. (D) i and ii, western blot showing expression of PP4 subunits across a panel of ovarian cancer cell lines. mRNA, messenger RNA; PP4, protein phosphatase 4; TCGA, The Cancer Genome Atlas.

regulatory subunits (online supplemental figure 1B). To assess the utility of targeting the PP4 complex in OC we next evaluated the expression levels of PP4 subunits in the OC TCGA data set. Using RNA-seq data, we found that *PPP4C* is significantly overexpressed in OC as compared with normal ovary and fallopian tube tissues (figure 1C), while the expression levels of the regulatory subunits were found to be variable (figure 1C). Increased mRNA expression was noted for *PPP4R3B* and *PPP4R2*. In contrast, *PPP4R3A* was found to be higher in normal tissue (figure 1C). At the protein level, PP4C was found to be robustly expressed across a panel of representative high grade serous ovarian cancer (HGSOC) cell lines (figure 1D, panel i). We obtained *PPP4C* RNA expression values and proteomic scores for relevant HGSOC cell lines from the DepMap portal. Both RNA level expression and proteome scores were consistent with the immunoblot data (online supplemental figure 1C). Interestingly, we noted variable expression of the PPP4R3β regulatory subunit across the OC cell lines, with TYK-nu and 59M showing the lowest expression (figure 1D, panel i). A similar trend was also observed with the other two regulatory subunits, PPP4R3α and PPP4R2 (figure 1D, panel ii). The major genetic mutations in the DDR and cell cycle pathways are summarized in online supplemental table 5. Overall, our data suggests that PP4C is frequently upregulated in OC.

Gene silencing or pharmacological inhibition of PP4C enhances sensitivity to carboplatin in OC

Given the known role of PP4 in the DDR, we next sought to ascertain the effect of PP4 inhibition on sensitivity to carboplatin, which is commonly used clinically in OC. *TP53* mutations are prevalent and are found in ~90% of all OC. As ID8 is a p53 wild-type cell line, we generated a p53 knockout ID8 cell line model using CRISPR. The gene edits in the targeted region were verified by Sanger sequencing and loss of p53 expression in the knockout clone was verified by western blot (online supplemental figure 2A-C). *PPP4C* knockdown with siRNA in ID8-p53WT and ID8-p53KO showed that loss of PP4C expression led to increased sensitivity to carboplatin in both the cell lines (figure 2A). PP4C expression after siRNA transfection was verified by western blot (figure 2A, inset). As an orthogonal approach, we generated ID8-p53KO cells with PP4C stable knockdown. In concordance to siRNA results, ID8-p53KO cells with low PP4C expression were found to be increasingly sensitive to carboplatin treatment when compared with vector control or parental cells (figure 2B). A western blot confirming PP4C expression after antibiotic selection is shown (figure 2B, inset). Similarly, treatment with pharmacological inhibitor of PP4, fostriecin, at nanomolar levels also resulted in enhanced sensitivity to carboplatin in ID8 mouse cell line (figure 2C). Decreased colony-forming capacity was seen on treatment with fostriecin and carboplatin in ID8-p53KO and the human OC cell lines, OVCAR3 and OVCAR8, compared with carboplatin treatment alone (figure 2D,E). These findings demonstrate that suppressing PP4 activity can lead to increased carboplatin sensitivity in OC. Additionally, we confirmed that PP4 phosphatase activity was inhibited by fostriecin in OVCAR3 and OVCAR4 human OC cell lines (online supplemental figure 3). Fostriecin is reported to inhibit PP4 at nanomolar concentrations.[30] However, to confirm that fostriecin is bound to PP4 at nanomolar levels leading to its inhibition, we performed a cellular thermal shift assay (CETSA). CETSA relies on the principle that when a drug binds to its target, it results in thermodynamic stabilization of the protein.[25] Our results show that fostriecin treatment increased the thermal stability of PP4C protein, which confirmed that PP4C is a direct target of fostriecin in OC cell lines (figure 2F).

Inhibition of PP4C enhances carboplatin induced DNA damage

Genomic instability is a hallmark of cancer. Deficiencies in the DDR can lead to genomic instability and can make cancer cells more sensitive to chemotherapy. Replication stress caused by chemotherapeutics that induce double-strand breaks, such as carboplatin, can lead to micronuclei formation, a manifestation of genomic instability. We found that PP4 inhibition with fostriecin combined with carboplatin led to increased micronuclei formation in multiple OC cell lines (figure 3A; online supplemental figure 4A). As PP4 has a known role in DDR, we sought to determine if fostriecin treatment affected H2AX (S139) phosphorylation (γ-H2AX), which is a well-reported substrate for PP4 phosphatase.[14] Our results show that fostriecin treatment in combination with carboplatin increased the number of γ-H2AX foci (figure 3B), γ-H2AX foci intensity, and overall γ-H2AX levels in OC cells (online supplemental figure 4B). However, we did not observe any significant changes in γ-H2AX with fostriecin treatment alone (online supplemental figure 4B). Since carboplatin is known to induce interstrand crosslinks (ICLs), we next investigated whether FANCD2 foci, a critical sensor of ICLs,[31] were altered by PP4 inhibition. Consistent with literature, we found increased FANCD2 foci in response to carboplatin treatment. However, fostriecin treatment did not increase the number of FANCD2 foci per cell (figure 3B) and no difference was observed in FANCD2 foci intensity with addition of fostriecin to carboplatin treated cells (online supplemental figure 4C). Because PP4 is known to play a role in HR,[13] we next determined whether loss of PP4 affects HR activity in OC cells. For this, we utilized OVCAR8-DR-GFP cells, which have a chromosomally integrated DR-GFP construct. The DR-GFP construct has two dysfunctional copies of the GFP gene, one copy is made defective by the insertion of 18 bp recognition sequence for I-SceI endonuclease (SceGFP) while the other copy is truncated at both ends (iGFP). When cells are transfected with pCßASceI, a double stranded break is generated in this construct, which can then be repaired only by HR. HR-mediated DNA repair gives rise to a functional GFP gene resulting in GFP expression, which can then

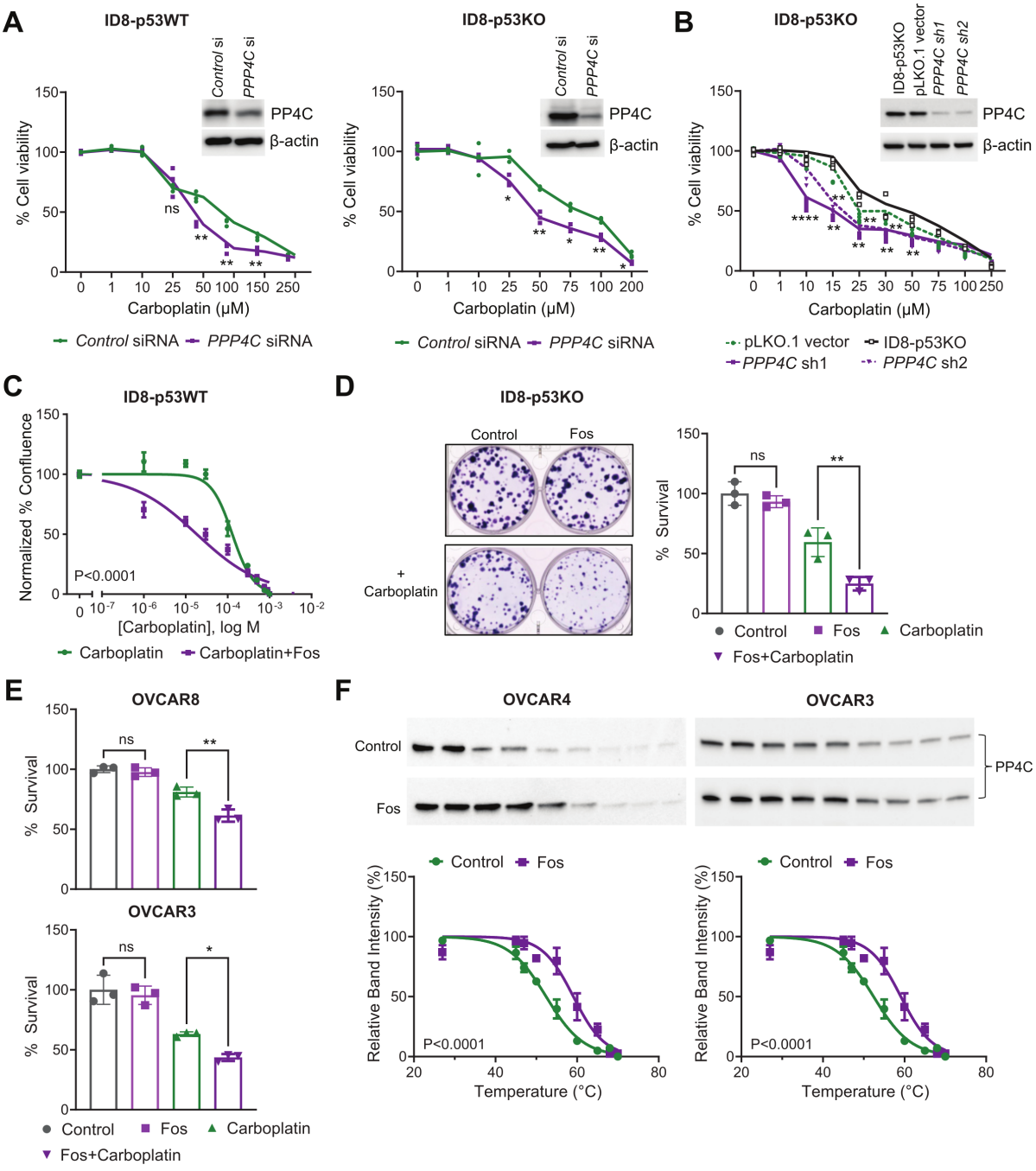

Figure 2 PP4 inhibition or knockdown sensitizes ovarian cancer cell lines to carboplatin. (A) The mouse ovarian cancer cell line, ID8 (ID8-p53WT) and the isogenic p53 knockout cell line (ID8-p53KO) were transfected with control or *PPP4C* siRNA. Cell viability was measured by MTS assay at 96 hours. Results represent three replicates per experiment group, mean±SEM, *p<0.05, **p<0.01. PP4C knockdown following siRNA transfection was verified by western blot (inset). (B) ID8-p53KO cells were stably transduced with two shRNA constructs targeting *PPP4C* or control plasmid using lentivirus. The stable cell lines were treated with increasing doses of carboplatin and cell viability was determined at 96 hours by MTS assay. Western blot confirming the reduction in PP4 expression in shRNA transfected cell lines compared with vector control is shown (inset) (C) ID8-p53WT cells were pretreated±fostriecin (Fos) (1 nM) for 24 hours, followed by carboplatin treatment at the indicated doses. Cell proliferation was monitored using Incucyte S3 and the difference in mean cell confluence across treatment groups (n=6) is plotted, *p<0.0001. (D) Clonogenic survival assay of ID8-p53KO cells pretreated±Fos (1 nM), followed by carboplatin (10 μM) treatment, mean±SEM, ns, not significant, **p<0.01. Representative images are shown adjacent to the graph. (E) Human ovarian cancer cell lines OVCAR8 and OVCAR3 cells were pretreated±Fos (1 nM), followed by carboplatin (1 μM) and colony formation was determined. Mean values are shown from three independent experiments. Error bars show SEM for each group, *p<0.05, **p<0.01. (F) Cellular thermal shift assay assay with OVCAR4 and OVCAR3 cells±Fos (10 nM). The increase in protein stability was determined by western blot. Relative band intensities were calculated from images and represented as percentage relative to control. Data shown is an average of three biological replicates, *p<0.0001. MTS, 3-(4,5-dimethylthiazol-2-yl)-5-(3-carboxymethoxyphenyl)-2-(4-sulfophenyl)-2*H*-tetrazolium; PP4, protein phosphatase 4.

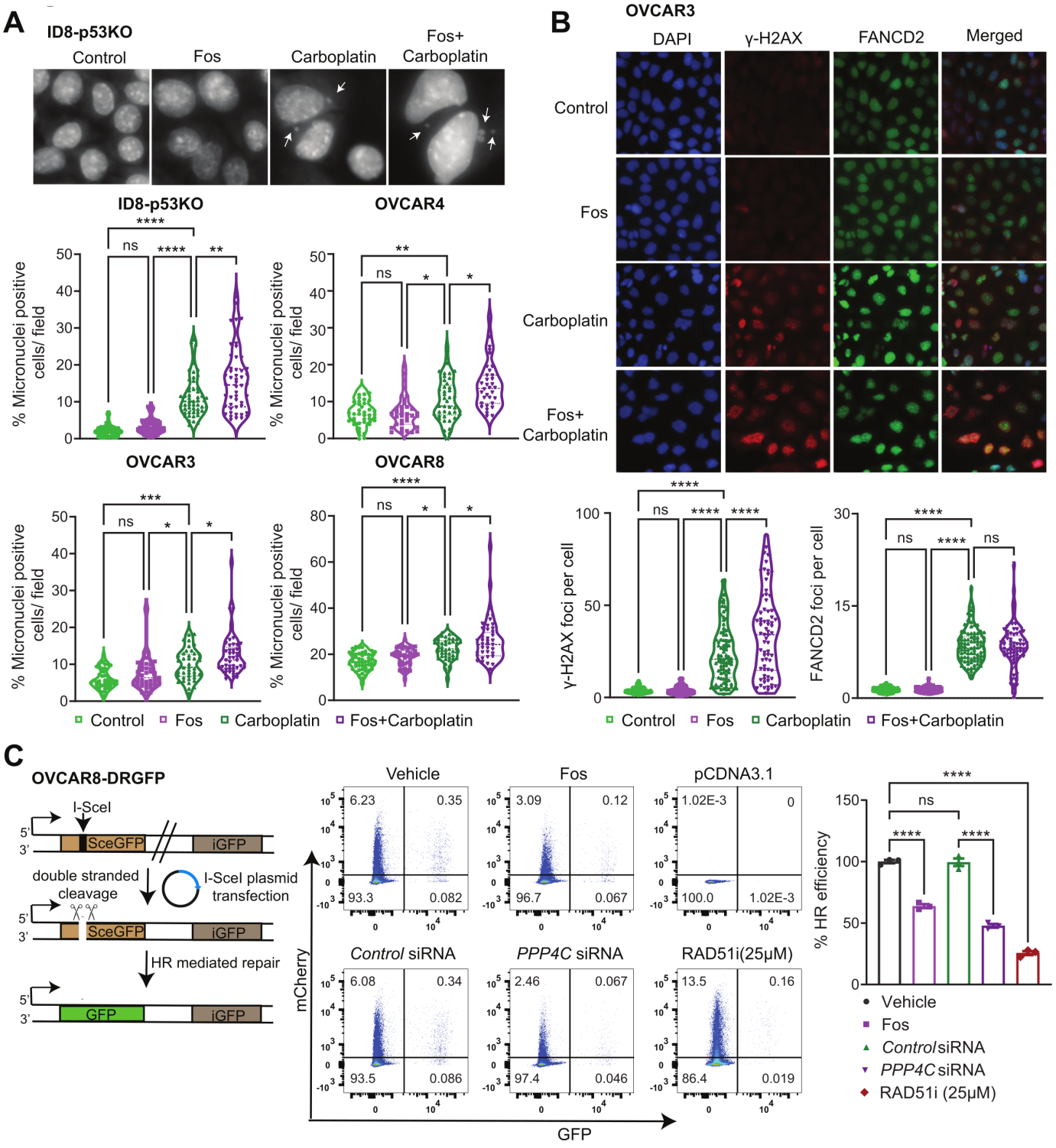

Figure 3 Pharmacological inhibition of PP4 augments carboplatin-induced DNA damage. (A) Ovarian cancer cell lines were pretreated with Fos (1 nM) for 24 hours followed by carboplatin at indicated doses, ID8-p53KO (10 μM), OVCAR4 (1 μM), OVCAR3 (1 μM), and OVCAR8 (2.5 μM). At 96 hours, micronuclei formation was quantified. Representative micrographs from ID8-p53KO cells depicting micronuclei are shown. The micronuclei count per 45–50 sites was averaged across conditions and represented as violin plots,*p<0.05, **p<0.01, **p<0.001, ****p<0.0001. (B) OVCAR3 cells were pretreated±Fos (1 nM), followed by carboplatin treatment at 2.5 μM for 96 hours and co-immunostained with FANCD2 and γ-H2AX. Representative images of γ-H2AX and FANCD2 foci across treatment conditions are shown. Image-based quantitation of foci counts was done across 70–90 sites and are shown in violin plots. ns, not significant, ****p<0.0001. (C) Left, schematic of DR-GFP assay. Right, representative flow plots showing GFP expression in OVCAR8-DR-GFP cells following transfection with pCβASceI plasmid and indicated treatment conditions. pCDNA3.1 was used as a transfection control. The percentage of cells expressing GFP fluorescence were quantified and efficiencies in homologous recombination were normalized to either untreated controls or control siRNA transfected cells. Values are mean+SEM. ***p<0.001, ****p<0.0001. Fos, fostriecin; PP4, protein phosphatase 4.

be quantified.[32] Cells treated with the RAD51 inhibitor, B-02, were used as a positive control. *PPP4C* knockdown via siRNA or fostriecin treatment inhibited HR as shown using the DR-GFP cell line (figure 3C). These data demonstrate that inhibition of PP4 leads to increased DNA damage and markers of genomic instability in OC cell lines following treatment with carboplatin.

PP4 inhibition promotes inflammatory signaling in OC

The presence of cytosolic DNA such as micronuclei can lead to activation of the cyclic GMP-AMP synthase (cGAS)-stimulator of interferon genes (STING) pathway, which can trigger pro-inflammatory signaling and synergize with immunotherapy to promote antitumor immunity.[33] Due to the increase in micronuclei observed with PP4 inhibition (figure 3A), we hypothesized that inflammatory signaling would be increased in OC cells on loss of PP4 activity. Signal transducer and activator of transcription (STAT) 1 is a key mediator of IFN signaling and plays an important role in both innate and adaptive immunity.[34] STAT1 phosphorylation at Y701 is essential for its activation and nuclear translocation. Additional phosphorylation at S727 is required for full transcriptional activation of STAT1. We found that treatment with the combination of fostriecin and carboplatin led to increased STAT1 (Y701) phosphorylation in OC cell lines as compared with carboplatin treatment alone (figure 4A, online supplemental figure 5A). Similar to fostriecin treatment, knockdown of *PPP4C* combined with carboplatin also resulted in increased STAT1 activation in OC cell lines (figure 4B, online supplemental figure 5B). The loss of perinuclear envelope surrounding the micronuclei, can trigger pattern recognition receptor cGAS, which in turn elicits STING-mediated type I IFN response resulting in STAT1 phosphorylation.[35] STING activates several transcription factors including Interferon regulatory factor (IRF) 3 and NF-κB leading to the production of type I IFN and pro-inflammatory cytokines.[36] Consistent with literature, we observed significant upregulation of phospho-p65 in response to fostriecin and carboplatin in both OVCAR3 and OVCAR8 cells (figure 4C). Canonical NF-kB (p65) was also found to be activated on knockdown of *PPP4C* expression via siRNA combined with carboplatin treatment (figure 4D). As we observed increased phospho-p65 in response to PP4C loss and carboplatin treatment, we next determined the levels of *IFNB1* and selected pro-inflammatory chemokines and cytokines in OC cells. At the mRNA level, *IFNB1, CCL5, CXCL10,* and *IL-6* were found to be increased with the combination treatment of carboplatin with fostriecin (online supplemental figure 5C,D) or *PPP4C* siRNA (figure 4E, online supplemental figure 5E). In addition, we performed a cytokine array with the conditioned media collected from carboplatin treated OVCAR3 cells, which were transfected with either control or *PPP4C* siRNA. We observed a clear induction in protein level expression of IL-6 and CXCL10 on loss of PP4C and carboplatin treatment, which was consistent with the increase observed at the mRNA level. Moreover, we also observed increased expression of additional senescent-associated secretory phenotype (SASP)-related cytokines including IL-8, CCL2, TNF-α, and CXCL9 with PP4C knockdown (figure 4F). Collectively, these data demonstrate that PP4 inhibition augments carboplatin-induced inflammatory signaling in OC cell lines.

PP4 inhibition in OC cells boosts immune cell migration via the STING pathway

Previous studies have shown that increased CD8 T-cell infiltration correlated with improved prognosis in OC.[4] CCL5, CXCL9, and CXCL10 have been shown to enhance both T and NK cell infiltration into tumors.[37 38] To determine whether pro-inflammatory cytokines and chemokines produced on combination of carboplatin and PP4 inhibition influences immune cell migration, we collected conditioned media from both mouse and human OC cell lines following treatment with fostriecin and carboplatin. Mouse OT-I CD8 T cells or NK-92 cells were placed in a Boyden chamber with either the mouse or human OC conditioned media, respectively, (figure 5A, schematic). Both mouse CD8 T cells and NK-92 cells displayed enhanced migration when exposed to conditioned media from OC cells treated with the combination of fostriecin and carboplatin (figure 5A). Additionally, we verified that direct fostriecin treatment had no effect on T-cell viability and did not negatively influence chicken ovalbumin (OVA)-induced T-cell activation as shown by intracellular cytokine staining for IFN-γ and TNF-α (online supplemental figure 6A).

We next sought to determine whether blocking signaling downstream of chemokine and cytokine receptors could blunt the immune cell migration induced by the conditioned media from carboplatin and fostriecin treated OC cells. Consistent with the well-documented role of Rac signaling in chemokine-induced cell migration,[39] we observed a significant reduction of both CD8 T and NK cell migration in the presence of an Rac inhibitor (figure 5B). However, we observed cell-type specific responses to MEK and STAT3 inhibitors. The STAT3 inhibitor, Stattic, suppressed CD8 T-cell migration but increased NK-92 cell migration (figure 5B). These results are consistent with previous reports as STAT3 signaling is known to be activated in migrating CD8 T cells in response to IL-6,[40] whereas STAT3 is reported to have an opposing effect on NK cell migration.[41] Similar to STAT3 signaling, MEK inhibition also resulted in distinct cellular responses from CD8 T and NK cells. Interestingly, the MEK inhibitor suppressed NK cell migration, whereas CD8 T-cell migration remained unaffected (figure 5B). To determine if cGAS-STING signaling played a role in the observed increase in T and NK cell migration, we knocked down *STING1* using siRNA in OVCAR8 cells (online supplemental figure 6B). Conditioned media from *STING1* knockdown OVCAR8 cells failed to stimulate human CD8 T-cell migration following PP4 inhibition (figure 5C). These data show that the pro-inflammatory

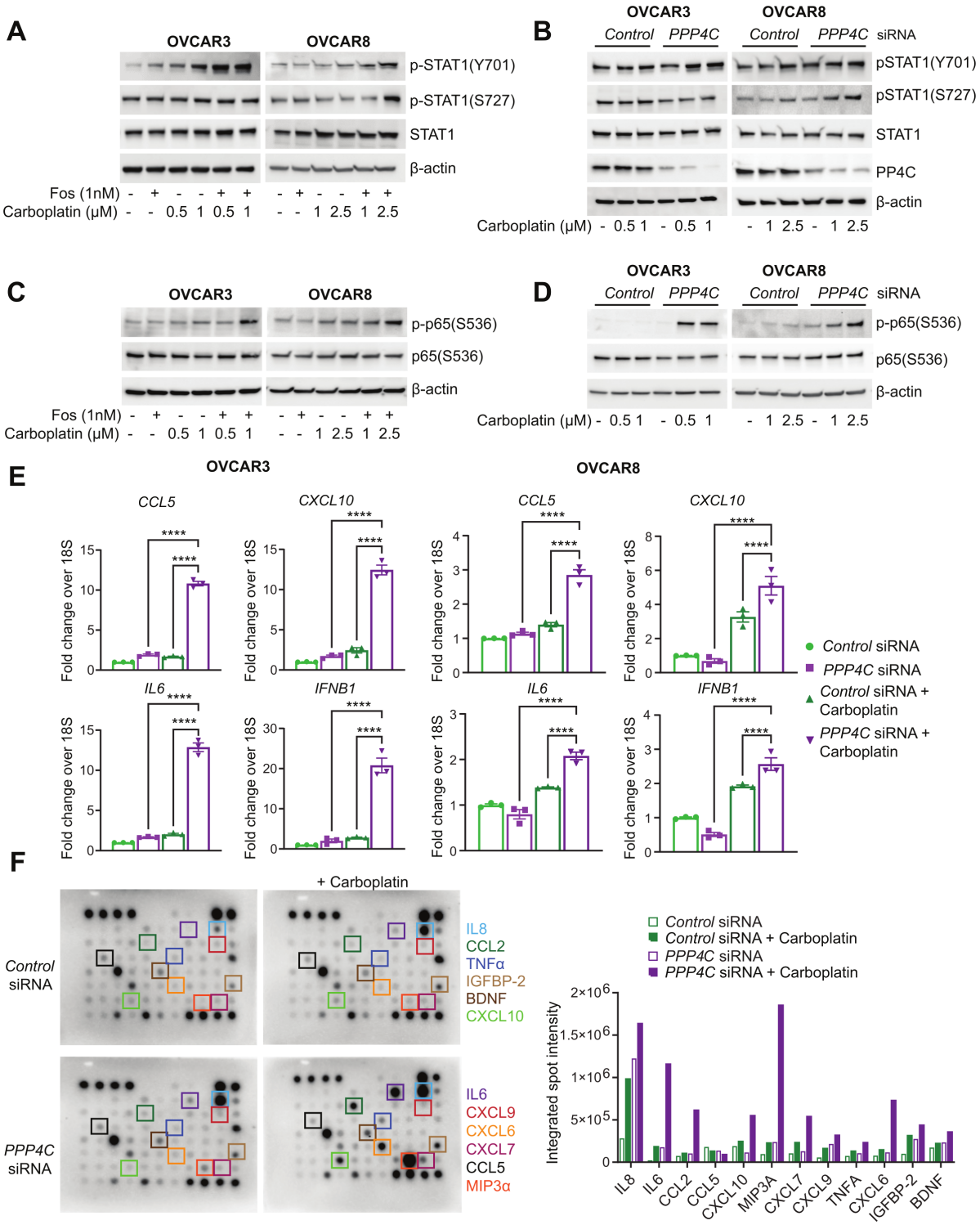

Figure 4 Loss of PP4 activity potentiates DNA damage-induced inflammatory signaling. (A) Representative western blot showing STAT1 phosphorylation at Y701 and S727 in OC cells pretreated±Fos (1 nM) for 24 hours followed by carboplatin treatment at the indicated doses on day 5. (B) STAT1 signaling shown following *PPP4C* siRNA transfection and carboplatin treatment on day 5. PP4C expression is also shown. (C) Representative western blot showing p65 phosphorylation at S536 in OC cells pretreated±Fos (1 nM) for 24 hours followed by carboplatin treatment at indicated doses on day 5. (D) Immunoblots of p-p65 following PPP4C siRNA transfection and carboplatin treatment on day 5. Actin is used as loading control. (E) RNA transcript levels of *CCL5*, *CXCL10*, *IL-6* and *IFNB1* were measured in OVCAR3 (left) and OVCAR8 (right) cells±*PPP4C* siRNA transfection and carboplatin treatment by quantitative, real-time PCR and relative fold change was calculated from three replicates. Values are mean±SEM. *p<0.05, **p<0.01, ***p<0.001 and ****p<0.0001. (F) Cytokine array analysis with conditioned media collected from OVCAR3 cells transfected with either *control* or *PPP4C* siRNA±carboplatin. Spot densities of select cytokines are shown. Fos, fostriecin; OC, ovarian cancer; PP4, protein phosphatase 4; STAT, signal transducer and activator of transcription.

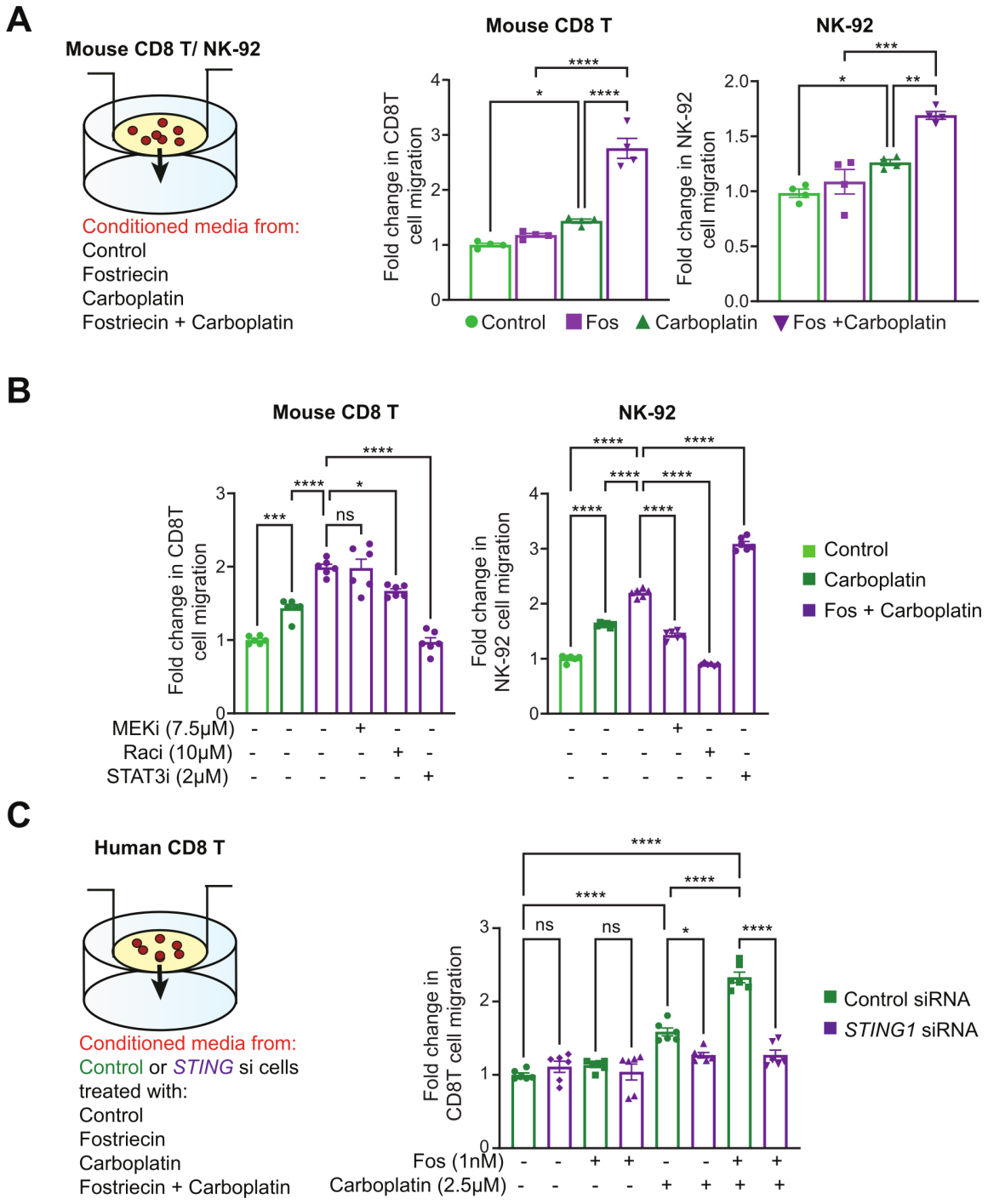

Figure 5 Protein phosphatase 4 knockdown in ovarian cancer cells enhances effector immune cell migration. (A) Left, schematic diagram of in vitro immune cell migration assay. Conditioned media was collected on day 5 from either ID8-p53KO (mouse) or OVCAR3 (human) cells pretreated±Fos for 24 hours followed by carboplatin treatment at the indicated doses: 10 μM (ID8-p53KO) and 1 μM (OVCAR3). The conditioned media from each treatment group was loaded in the bottom chamber. Right, fold change in migration was calculated relative to control, mean±SEM (n=3) is shown. *p<0.05, **p<0.01, ***p<0.001 and ****p<0.0001. (B) Conditioned media was collected on day 5 from either ID8-p53KO or OVCAR3 cells that were treated as described in (A). In parallel, CD8 T or NK-92 cells were pretreated with either MEKi (7.5 μM) or Raci (10 μM) or STAT3i (2 μM) for 15 min prior to adding in the transwell chamber. Conditioned media from each treatment group was loaded in the bottom chamber. Fold change in migration was calculated relative to control, mean±SEM (n=3) is shown. *p<0.05, ***p<0.001 and ****p<0.0001. (C) Left, schematic diagram of *in vitro* CD8 T-cell migration assay following *STING1* siRNA transfection in ovarian cancer cells. OVCAR8 cells were transfected with control or *STING1* siRNA±Fos and carboplatin. On day 5, conditioned media was collected and used in the lower chamber as chemoattractant. Human CD8 T cells were isolated from the ascites of a patient with ovarian cancer and used in the upper chamber. Right, fold change in migration (n=3) is shown, ns, not significant, *p<0.05 and ****p<0.0001. Fos, fostriecin; NK, natural killer; STAT, signal transducer and activator of transcription; STING, stimulator of interferon genes.

signaling stimulated by PP4 inhibition is mediated by STING activation in OC cells.

PP4C knockdown in tumor cells augmented NK cell activation and cytotoxicity against OC

Since inhibition of PP4 activity led to increased inflammatory signaling and immune cell migration, next we examined whether PP4 subunit expression in OC correlates with immune cell infiltration using the TIMER V.2.0. Gene expression deconvolution algorithms CIBERSORT (cell type identification by estimating the relative subset of known RNA transcripts) and xCell were used to estimate the NK cell, CD8 T cell, and NK T-cell subsets based on bulk RNA-seq gene expression data from OC (TCGA). High transcript-level expression of *PPP4R3A* (SMEK1) and *PPP4R2* in OC correlated with a small but significant decrease in activated NK cell (CIBERSORT) and NK T (xCell) infiltration. We observed a similar negative correlation in NK (p value not significant) and NK T-cell filtration (p value significant) with high tumoral *PPP4R3B* expression. However, while we observed a negative trend with *PPP4C* expression, the adjusted p value did not reach statistical significance using CIBERSORT (online supplemental figure 7). There was no significant correlation between expression of PP4 subunits and CD8 T-cell infiltration (data not shown).

Studies have shown that OC is susceptible to NK cell-mediated killing and increased fractions of NK cells in ascites of patients with OC correlate with improved outcomes.[42 43] However, as we observed a significant negative correlation between RNA level expression of PP4 subunits and NK cell infiltration in OC, we next wanted to test our hypothesis that *PPP4C* or *PPP4R3B* knockdown can positively influence NK cell function against OC. We measured IFN-γ^+ effector NK cells following co-culture with NK-92 cells and OVCAR3 and OVCAR8 cells were transfected with either control, *PPP4C* or *PPP4R3B* siRNA. We saw a significant increase in IFN-γ^+ NK cells in response to either *PPP4C* or *PPP4R3B* knockdown as compared with the control that was further increased by carboplatin (figure 6A,B). We next assessed NK cell degranulation following a 3 hours co-culture between NK-92 cells and OVCAR8 cells transfected with control, *PPP4C*, or *PPP4R3B* siRNA. We saw a significant increase in CD107a$^+$ NK-92 cells in response to either *PPP4C* or *PPP4R3B* knockdown. We also observed a significant increase in CD107a$^+$ NK-92 cell population on co-culture with carboplatin treated cells (figure 6C). To further determine if the increase in NK cell activation and degranulation mediated by loss of PP4 contributed to an increase in NK cell-mediated OC cell killing, we co-cultured OC cell lines transfected with control, *PPP4C*, or *PPP4R3B* siRNA with NK-92 cells. Our results show that loss of *PPP4C* or *PPP4R3B* expression in OC enhances NK cell-directed OC cell killing (figure 6D). Carboplatin treatment induced a significant increase in killing with OVCAR8 cells, which was further increased in both PP4C and PPP4R3β knockdown cells (figure 6D). In OVCAR3, even though there was increased killing in carboplatin treated cells over the siRNA alone group, it did not achieve statistical significance (online supplemental figure 8A). We additionally confirmed that the killing observed was due to the addition of NK cells and not due to loss of PP4C or PPP4R3β expression. Our results show that knockdown of PPP4R3β did not significantly induce apoptosis in the absence of NK cells in either the OVCAR3 or OVCAR8 cell lines (online supplemental figure 8B). Silencing of PP4C resulted in a small but significant increase (11%–17.9%) in apoptosis in the OVCAR3 cell line, but not in the OVCAR8 cell line (online supplemental figure 8B).

Knockdown of PP4C in a syngeneic, immunocompetent mouse model of OC results in reduced tumor growth and increased effector immune cell infiltration

Next, we sought to evaluate the effect of PP4C knockdown on OC tumor growth. We developed ID8-p53KO cells with reduced expression of PP4C (figure 2B). *In vivo*, PP4C knockdown resulted in significantly reduced overall tumor growth (figure 7A,B). In addition, there was significant reduction in ascites formation in PP4C knockdown tumors compared with control (figure 7C). To mimic our *in vitro* findings, we used a low dose of carboplatin *in vivo*. This low dose of carboplatin (5 mg/kg) did not have any effect on either control or PP4C knockdown tumor growth. Next, we determined the cellular changes in tumor, spleen, peritoneal lymph nodes, and ascites (figure 7D–I, online supplemental figures 9, 10). We observed a significant increase in both NK cell (CD3$^-$ CD161$^+$) and NK T cell (CD3$^+$CD161$^+$) infiltration in PP4C shRNA tumors compared with control while carboplatin treatment showed no additional increase in either group (figure 7D,E). Consistent with increased infiltration, we also identified increased IFN-γ^+ NK cells (CD3$^-$CD161$^+$) in PP4C shRNA tumors (figure 7F). Furthermore, we saw a significant increase in CD4$^+$ T-cell numbers within PP4C shRNA tumors, which again were unaffected with carboplatin treatment (figure 7G). Interestingly, carboplatin treatment significantly increased intratumoral CD8$^+$ T-cell numbers in PP4C shRNA tumors, which was not observed with the control treated group (figure 7H). Additionally, we found that the CD4$^+$CD25$^+$ T-cell population, which is representative of regulatory T cells, remained unchanged across all groups (figure 7I). The changes in NK cell composition were specific to tumors as we did not observe any changes across groups in the spleen, lymph nodes, or ascites (online supplemental figure 9A-C). For CD8$^+$ and CD4$^+$ T cells, we observed a slight increase in overall cell numbers in the spleen from mice with PP4C shRNA tumors whereas the numbers remained unaffected within both peritoneal lymph nodes and ascites (online supplemental figure 9D,E). An increase in CD4$^+$CD25$^+$ T-cell population was also noted in the spleen from mice with PP4C shRNA tumors while there was no change observed across groups in lymph nodes and ascites (online supplemental figure 9F). These data demonstrate that

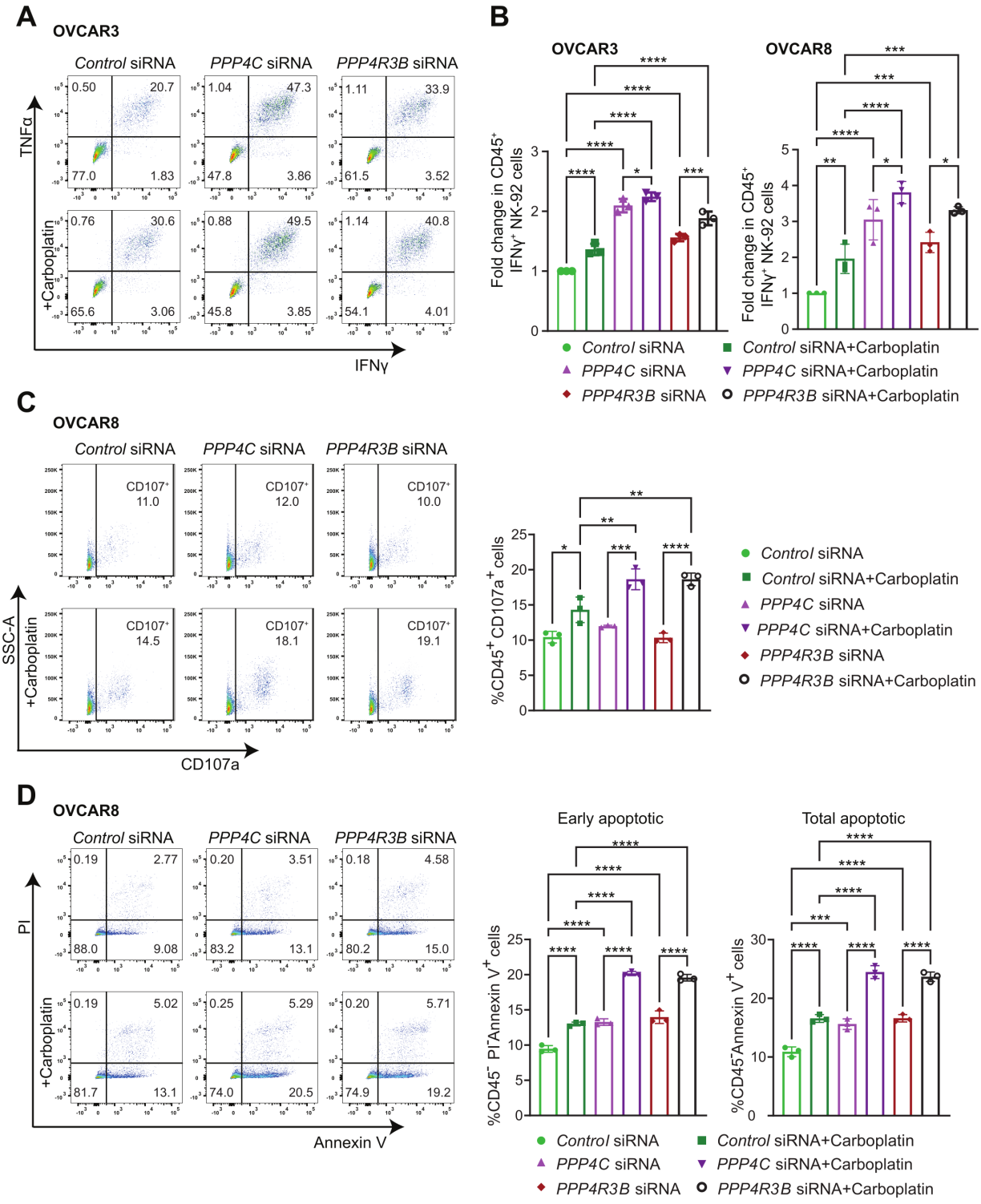

Figure 6 Loss of PP4 promotes NK cell activation and NK cell-directed ovarian cancer killing. OVCAR3 and OVCAR8 cells were transfected with either control or *PPP4C* or *PPP4R3B* siRNA, followed by carboplatin treatment at indicated doses: OVCAR3 (0.5 µM), OVCAR8 (2.5 µM). On day 5, cells were co-cultured with NK-92 (1:1) and immunostained for IFN-γ and TNF-α following PMA restimulation. (A) representative scatter plots of the cytokine production in OVCAR3 are shown. (B) relative fold changes in IFN-γ+ cells were calculated for OVCAR3 (n=3) and OVCAR8 (n=3), mean±SD is shown, *p<0.05, **p<0.01, ***p<0.001 and ****p<0.0001. (C) Left, representative flow scatter plots and, right, the percentage of $CD45^+$ $CD107a^+$ cells following NK-92 and OVCAR8 co-culture are shown as bar graph, ***p<0.001 and ****p<0.0001 (D) NK-92 mediated cytotoxicity assays. OVCAR8 cells (n=3) were transfected with control or *PPP4C* or *PPP4R3B* siRNA±carboplatin treatment (2.5 µM). NK-92 cells were added in a 1:1 ratio. After 3 hours, the cells were stained with annexin V and PI and the CD45-negative cells were analyzed. Representative flow plots and percentage of early and total apoptotic cells are shown for all treatment groups, mean±SD, ****p<0.0001. IFN, interferon; NK, natural killer; PI, propidium iodide; PMA, phorbol 12-myristate 13-acetate; PP4, protein phosphatase 4; SSC-A, side scatter-area; TNF, tumor necrosis factor.

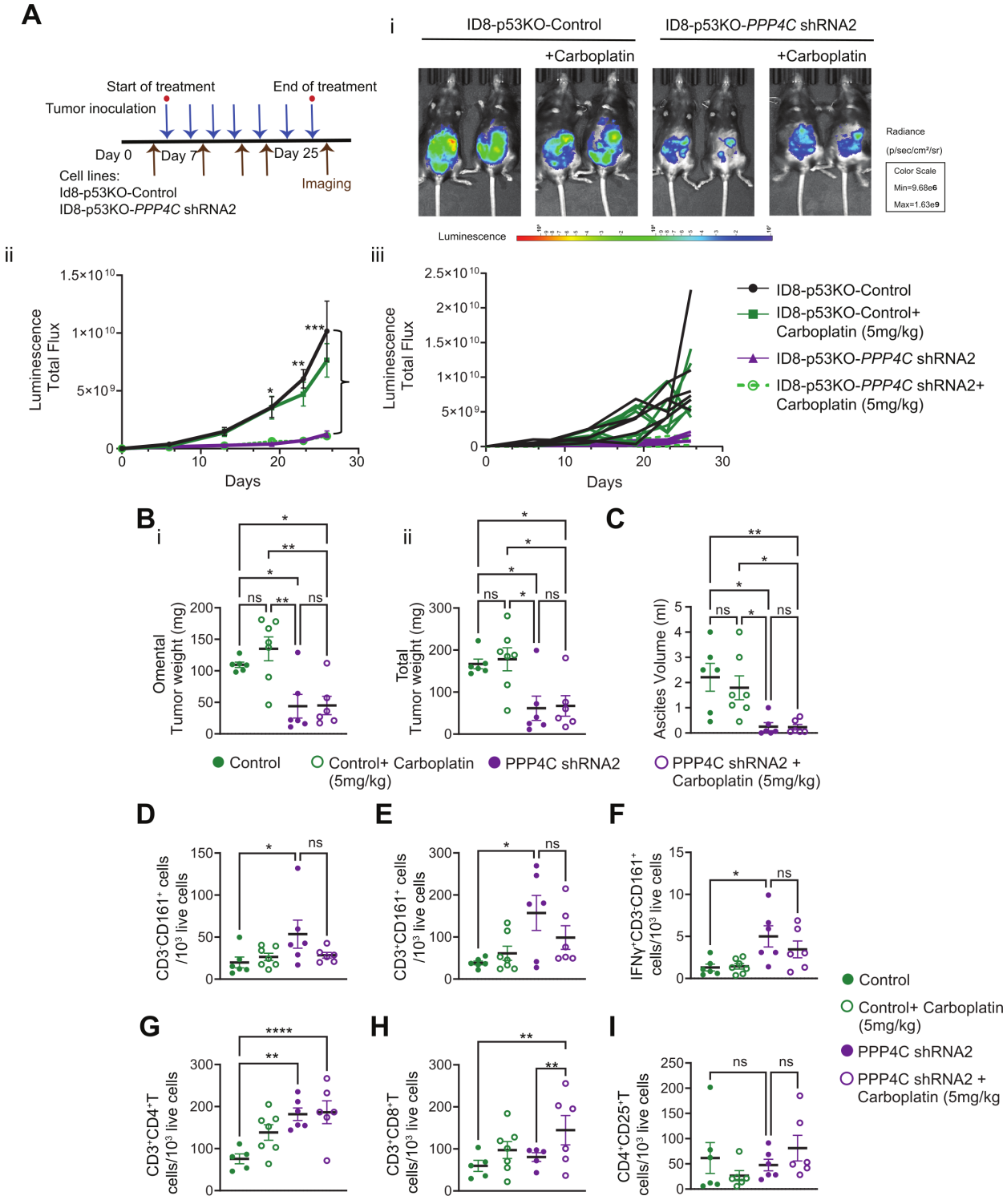

Figure 7 PP4C knockdown augments immune cell infiltration. (A) Left, schematic. Immune proficient C57BL/6 mice were injected with ID8-p53KO control and ID8-p53KO-ppp4shRNA clone 2 cells (n=6–7 mice). (i) Representative images for mice from respective groups showing relative tumor burden on day 26. (ii) Tumor growth was monitored by weekly measurement of luminescence (total flux) using IVIS, mean±SEM, *p<0.5, **p<0.01, ***p<0.001. (iii) Luminescence curves of individual mice measured over time. (B) i–ii, Primary omental tumor along with metastatic nodules were collected at time of necropsy, weighed, and shown as a bar graph, mean±SEM, *ns, not significant, p<0.05, **p<0.01. (C) Volume of ascites collected at necropsy is shown, ns, not significant, *p<0.05, **p<0.01. Tumors were disassociated and immune cell populations were identified by flow cytometry. (D, E) $CD3^{-}CD161^{+}$ and $CD3^{+}CD161^{+}$ per 10^{3} live cells, mean±SEM, ns, not significant, *p<0.05. (F) Quantitation of IFN-γ in CD3–CD161+natural killer cells following *ex vivo* restimulation with PMA/ionomycin for 4 hours, mean±SEM, ns, not significant, *p<0.05. (G, H) $CD4^{+}$ and $CD8^{+}$ T cells per 10^{3} live cells, mean±SEM, **p<0.01, ****p<0.0001. (I) $CD4^{+}CD25^{+}$ Treg population per 10^{3} live cells, mean±SEM, IFN, interferon; IVIS, *in vivo* imaging system; ns, not significant; PMA, phorbol 12-myristate 13-acetate; PP4, protein phosphatase; Treg, regulatory T cell; .

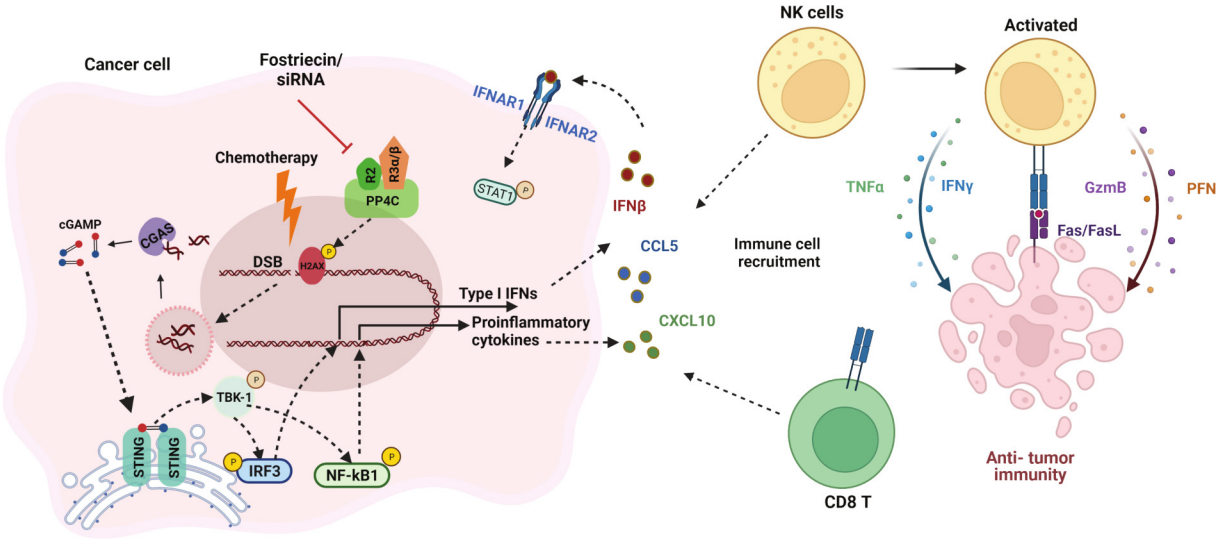

Figure 8 Schematic diagram showing mechanism by which PP4C is involved in antitumor immunity. Loss of PP4 augments chemotherapy-induced DNA damage triggering a type I interferon response mediated by STING and STAT1 signaling. Increased chemokine production on inhibition or knockdown of PP4C led to improved immune cell migration both *in vitro* and *in vivo* and augmented natural killer cell-directed ovarian cancer cell killing *in vitro*. Created with Biorender.com. cGAS, cyclic GMP-AMP synthase; DSB, double strand break; Gzm, granzyme; IFN, interferon; IRF, interferon regulatory factor; NF-κB, nuclear factor kappa B; PFN, perforin; PP4, protein phosphatase 4; STAT, signal transducer and activator of transcription; STING, stimulator of interferon genes; TNF, tumor necrosis factor.

PP4C knockdown reduces tumor burden and enhances immune effector cell tumor infiltration.

DISCUSSION

In this study, we provide direct evidence that loss of PP4 can augment inflammatory responses in OC caused by chemotherapy (figure 8, summary figure). Our results show that knockdown or pharmacological inhibition of PP4C activates type I IFN signaling leading to increased transcription of pro-inflammatory cytokines and STAT1 activation. Increased chemokines and cytokines from carboplatin treated, PP4-silenced OC cells enhanced immune cell migration in a STING-dependent manner. In addition, knockdown of either the catalytic subunit or regulatory subunit of PP4 in OC cells improved NK cell activation and NK cell-mediated OC killing. *In vivo*, loss of PP4C led to reduced tumor growth with increased effector immune cell infiltration. These findings support the further development of PP4 inhibitors to enhance the antitumor immune response in OC.

Clinical trials have revealed that single agent ICB therapy is not effective in patients with OC.[44] However, recent studies have highlighted that inhibition of the DDR can enhance immunogenicity and increase responses to ICB therapy.[45 46] Recent results from a phase II clinical study that combined pembrolizumab with the PARP inhibitor, niraparib, demonstrated an overall response rate (ORR) of 18% for all patients with OC,[8] which is higher than the ORR of 8% with pembrolizumab alone. In this trial, patients with *BRCA1/2* mutated tumors had the same response rate as those with wild-type tumors. This suggests that there are additional factors influencing the response to ICB beyond *BRCA1/2* and that combining ICB with modulators of DDR may be beneficial for those with OC. Previous studies have established that the multisubunit phosphatase complex, PP4, plays a significant role in the DDR through the dephosphorylation of several proteins that play integral roles in HR and/or NHEJ: γH2AX,[14] Kap-1/TRIM28,[16] RPA2,[13] and 53BP1.[15 47] PP4C, PPP4R2, and PPP4R3α (three components of PP4 complex) have been found to be significantly overexpressed in lung and breast cancers.[48] Our findings indicate that loss of PP4 activity in OC cells results in cancer cell-extrinsic immune cell activation. However, further studies are needed to determine whether PP4 inhibition influences ICB response in cancers with PP4 overexpression.

We had previously discovered that CT45 binds to and inhibits PP4, thereby enhancing carboplatin sensitivity.[17] Previous studies have also shown that when PP4 subunits were transiently silenced, resolution of the DNA damage was delayed, causing enhanced sensitivity to DNA damage-inducing agents. In this study we used a PP4 inhibitor, fostriecin. Fostriecin is a commercially available phosphate ester produced by *Streptomyces pulveraceous* that was originally identified as an antitumor antibiotic that demonstrated antitumor function in xenograft mouse models.[49] Subsequently it was discovered that fostriecin was a potent, selective inhibitor of PP4 and PP2 phosphatases.[50] Notably, many of the effects of fostriecin have more recently been attributed to its inhibition of PP4 rather than PP2A.[51] In addition, many OC tumors express high levels of the endogenous PP2A inhibitor, CIP2A,[52] and therefore, PP2A activity is anticipated to be low in the majority of OC tumors. In our study, fostriecin and *PPP4C*

siRNA combined with carboplatin induced overlapping phenotypes suggesting that fostriecin's main effects in OC are mediated by PP4 inhibition. Targeted inhibition of PPP Ser/Thr phosphatases is still a challenge owing to the high degree of active site conservation among this protein superfamily. Fostriecin did enter a phase I clinical trial in the early 2000s but the study was terminated due to issues with purity and supply of the drug.[53 54] Efforts have been taken to combat these issues, including the development of fostriecin analogs or fostriecin-like inhibitors.[50 55] Future development of PP4-specific inhibitors will be needed to define the clinical utility of these types of inhibitors for OC.

Genomic instability can trigger antitumor immunity through recognition of cytosolic DNA by cGAS and subsequent activation of the STING pathway.[56] Activation of the cGAS-STING pathway leads to inflammatory signaling through activation of transcription factors IRF3 and NF-κB.[57] Both host[58] and tumor intrinsic[59] STING activation have been shown to be important for the antitumor immune response and response to ICB. Here, our results show increased canonical NF-κB activation and the upregulation of multiple inflammatory genes including *CCL5*, *CXCL9*, *CXCL10*, *IL-6* as well as *IFNB1*, following carboplatin treatment and PP4 inhibition in OC cells. Increased production of CXCL9 and CXCL10 have been shown to be associated with increased tumor immune infiltrates in OC as well as with improved response to therapy in melanoma, ovarian, and breast cancer.[60–62] Knockdown of STING in *PP4C* siRNA transfected OC cells, led to decreased immune cell migration *in vitro*, underscoring the role of STING in promoting an inflammatory phenotype following DNA damage in PP4-inhibited OC cells. At the protein level, we also found increased expression of several other cytokines including IL-8, TNF-α, CCL2, and MIP3α, that are correlated with the SASP phenotype.[63 64] The cGAS-STING pathway is a critical regulator of senescence and the SASP phenotype,[65] suggesting that PP4 inhibition may contribute to a pro-inflammatory, SASP phenotype through the cGAS-STING pathway in OC cells.

One of the key findings in our study is the demonstration of the functional effect of PP4 knockdown on NK cell activation, cytolytic activity, and tumor infiltration in OC. Interestingly, we found differences in the effect of *PPP4C* siRNA versus *PPP4R3B* siRNA on NK cell production of TNF-α/IFN-γ, which were not present with NK cell-directed OC cytotoxicity. Since the catalytic function of PP4 phosphatase activity is tightly regulated by its interaction with its regulatory subunits,[66] we expect that reduction of the catalytic subunit, PP4C, would have a more pronounced effect than reduction of one of the regulatory subunits, PPP4R3β. In addition, it is currently understood that NK cells mediate their cytolytic activity, through release of granzyme B and perforin, within minutes of encountering target cells[67] while production of TNF-α/IFN-γ has been shown to have slower kinetics.[68] Correlating with these results, we found increased tumor infiltration of IFN-γ-producing NK cells and NK T cells ($CD3^+CD161^+$) in PP4C shRNA tumors that was associated with reduced tumor burden. NK cells have been shown to be associated with improved overall survival in OC as well as in breast cancer and melanoma.[69–72] Increased IFN-γ production within the tumor microenvironment is known to lead to upregulation of major histocompatibility (MHC) class I antigen processing and presentation, which promotes the adaptive immune response. We also observed increases in $CD4^+$ T-cell infiltration in PP4C shRNA tumors and $CD8^+$ T-cell infiltration increased with the addition of carboplatin in PP4C shRNA tumors. Future studies are needed to elucidate which immune cell types are needed for tumor control in the context of PP4 deficiency and on the role of PP4 in the response to ICB.

In conclusion, this study highlights the crucial role of PP4 in antitumor immunity and the need for specific inhibitors for effective clinical translation. To our knowledge, this is the first report demonstrating that knockdown or pharmacologic inhibition of PP4 in cancer cells results in enhancement of immune effector cell migration, function, and tumor infiltration. In light of these findings, we believe PP4 to be an attractive therapeutic target in OC that warrants further investigation.

Acknowledgements We are grateful to Scott Kaufmann for valuable advice, Larry Karnitz for providing the OVCAR8 DR-GFP cell line, and Abhinav Acharya for providing the NK-92 cell line. Biorender.com was used to generate the study summary schematic in Figure 8. We would like to thank the Mayo Clinic Comprehensive Cancer Center, the Flow Cytometry Core, and the Department of Comparative Medicine Animal Facility, Arizona, for their support of this study.

Contributors MC conceived and designed the study. RR contributed to the study design, performed experiments, and drafted the manuscript. RR and CW performed flow cytometry and cellular thermal shift assay. RR, MC, and EYB performed mouse experiments. TER performed immunofluorescence staining and data analysis. ECU contributed to manuscript writing. PMM and KAB provided resources. MC, PMM and KAB reviewed and edited the manuscript. MC supervised the work and is responsible for the overall content as guarantor.

Funding This work was supported by the Department of Defense Ovarian Cancer Research Program—Early Career Investigator Award, W81XWH2110489 (MC).

Competing interests No, there are no competing interests.

Patient consent for publication Not applicable.

Ethics approval This study involves human participants and was approved by Mayo Clinic Institutional Review Board, reference number: 18-010082. Participants gave informed consent to participate in the study before taking part.

Provenance and peer review Not commissioned; externally peer reviewed.

Data availability statement Data are available upon reasonable request. All data relevant to the study are included in the article or uploaded as supplementary information.

ORCID iD

Marion Curtis http://orcid.org/0000-0002-7152-6929

REFERENCES

1 Siegel RL, Miller KD, Fuchs HE, *et al*. Cancer statistics, 2021. *CA Cancer J Clin* 2021;71:7–33.
2 Allemani C, Matsuda T, Di Carlo V, *et al*. Global surveillance of trends in cancer survival 2000-14 (CONCORD-3): analysis of individual records for 37 513 025 patients diagnosed with one of 18 cancers from 322 population-based registries in 71 countries. *Lancet* 2018;391:1023–75.
3 Galluzzi L, Chan TA, Kroemer G, *et al*. The hallmarks of successful anticancer immunotherapy. *Sci Transl Med* 2018;10. doi:10.1126/scitranslmed.aat7807. [Epub ahead of print: 19 Sep 2018].
4 Zhang L, Conejo-Garcia JR, Katsaros D, *et al*. Intratumoral T cells, recurrence, and survival in epithelial ovarian cancer. *N Engl J Med* 2003;348:203–13.
5 Sato E, Olson SH, Ahn J, *et al*. Intraepithelial CD8$^+$ tumor-infiltrating lymphocytes and a high CD8$^+$/regulatory T cell ratio are associated with favorable prognosis in ovarian cancer. *Proc Natl Acad Sci U S A* 2005;102:18538–43.
6 Kandalaft LE, Odunsi K, Coukos G. Immunotherapy in ovarian cancer: are we there yet? *J Clin Oncol* 2019;37:2460–71.
7 Ding L, Kim H-J, Wang Q, *et al*. PARP inhibition elicits STING-dependent antitumor immunity in BRCA1-deficient ovarian cancer. *Cell Rep* 2018;25:2972–80.
8 Konstantinopoulos PA, Waggoner S, Vidal GA, *et al*. Single-Arm phases 1 and 2 trial of Niraparib in combination with pembrolizumab in patients with recurrent platinum-resistant ovarian carcinoma. *JAMA Oncol* 2019;5:1141–9.
9 FDA. LYNPARZA prescribing information 2017 update 2014.
10 Shen J, Zhao W, Ju Z, *et al*. PARPi triggers the STING-dependent immune response and enhances the therapeutic efficacy of immune checkpoint blockade independent of BRCAness. *Cancer Res* 2019;79:311–9.
11 Wang Z, Sun K, Xiao Y, *et al*. Niraparib activates interferon signaling and potentiates anti-PD-1 antibody efficacy in tumor models. *Sci Rep* 2019;9:1853.
12 Park J, Lee D-H. Functional roles of protein phosphatase 4 in multiple aspects of cellular physiology: a Friend and a foe. *BMB Rep* 2020;53:181–90.
13 Lee D-H, Pan Y, Kanner S, *et al*. A PP4 phosphatase complex dephosphorylates RPA2 to facilitate DNA repair via homologous recombination. *Nat Struct Mol Biol* 2010;17): :365–72.
14 Chowdhury D, Xu X, Zhong X, *et al*. A PP4-phosphatase complex dephosphorylates gamma-H2AX generated during DNA replication. *Mol Cell* 2008;31:33–46.
15 Lee D-H, Acharya SS, Kwon M, *et al*. Dephosphorylation enables the recruitment of 53BP1 to double-strand DNA breaks. *Mol Cell* 2014;54:512–25.
16 Lee D-H, Goodarzi AA, Adelmant GO, *et al*. Phosphoproteomic analysis reveals that PP4 dephosphorylates KAP-1 impacting the DNA damage response. *Embo J* 2012;31:2403–15.
17 Coscia F, Lengyel E, Duraiswamy J, *et al*. Multi-Level proteomics identifies CT45 as a chemosensitivity mediator and immunotherapy target in ovarian cancer. *Cell* 2018;175:159–70.
18 Walton J, Blagih J, Ennis D, *et al*. CRISPR/Cas9-Mediated *Trp53* and *Brca2* Knockout to Generate Improved Murine Models of Ovarian High-Grade Serous Carcinoma. *Cancer Res* 2016;76:6118–29.
19 Cerami E, Gao J, Dogrusoz U, *et al*. The cBio cancer genomics portal: an open platform for exploring multidimensional cancer genomics data. *Cancer Discov* 2012;2:401–4.
20 Cline MS, Craft B, Swatloski T, *et al*. Exploring TCGA pan-cancer data at the UCSC cancer genomics Browser. *Sci Rep* 2013;3:2652.
21 Li T, Fu J, Zeng Z, *et al*. TIMER2.0 for analysis of tumor-infiltrating immune cells. *Nucleic Acids Res* 2020;48:W509–14.
22 Newman AM, Liu CL, Green MR, *et al*. Robust enumeration of cell subsets from tissue expression profiles. *Nat Methods* 2015;12:453–7.
23 Sturm G, Finotello F, Petitprez F, *et al*. Comprehensive evaluation of transcriptome-based cell-type quantification methods for immuno-oncology. *Bioinformatics* 2019;35:i436–45.
24 Guzmán C, Bagga M, Kaur A, *et al*. ColonyArea: an ImageJ plugin to automatically quantify colony formation in clonogenic assays. *PLoS One* 2014;9:e92444.
25 Jafari R, Almqvist H, Axelsson H, *et al*. The cellular thermal shift assay for evaluating drug target interactions in cells. *Nat Protoc* 2014;9:2100–22.
26 Curtis M, Kenny HA, Ashcroft B, *et al*. Fibroblasts mobilize tumor cell glycogen to promote proliferation and metastasis. *Cell Metab* 2019;29:141–55.
27 Kanakkanthara A, Huntoon CJ, Hou X, *et al*. ZC3H18 specifically binds and activates the BRCA1 promoter to facilitate homologous recombination in ovarian cancer. *Nat Commun* 2019;10): :4632.
28 Galeano Niño JL, Pageon SV, Tay SS, *et al*. Cytotoxic T cells Swarm by homotypic chemokine signalling. *Elife* 2020;9. doi:10.7554/eLife.56554. [Epub ahead of print: 13 Oct 2020].
29 Chava S, Bugide S, Gupta R, *et al*. Measurement of natural killer cell-mediated cytotoxicity and migration in the context of hepatic tumor cells. *J Vis Exp* 2020;156. doi:10.3791/60714. [Epub ahead of print: 22 Feb 2020].
30 Boger DL, Ichikawa S, Zhong W. Total synthesis of fostriecin (CI-920). *J Am Chem Soc* 2001;123:4161–7.
31 Lopez-Martinez D, Liang C-C, Cohn MA. Cellular response to DNA interstrand crosslinks: the Fanconi anemia pathway. *Cell Mol Life Sci* 2016;73:3097–114.
32 Pierce AJ, Johnson RD, Thompson LH, *et al*. XRCC3 promotes homology-directed repair of DNA damage in mammalian cells. *Genes Dev* 1999;13:2633–8.
33 Motwani M, Pesiridis S, Fitzgerald KA. DNA sensing by the cGAS-STING pathway in health and disease. *Nat Rev Genet* 2019;20:657–74.
34 Meissl K, Macho-Maschler S, Müller M, *et al*. The good and the bad faces of STAT1 in solid tumours. *Cytokine* 2017;89:12–20.
35 Harding SM, Benci JL, Irianto J, *et al*. Mitotic progression following DNA damage enables pattern recognition within micronuclei. *Nature* 2017;548:466–70.
36 Abe T, Barber GN. Cytosolic-DNA-mediated, STING-dependent proinflammatory gene induction necessitates canonical NF-κB activation through TBK1. *J Virol* 2014;88:5328–41.
37 Wennerberg E, Kremer V, Childs R, *et al*. CXCL10-induced migration of adoptively transferred human natural killer cells toward solid tumors causes regression of tumor growth in vivo. *Cancer Immunol Immunother* 2015;64:225–35.
38 Nagarsheth N, Wicha MS, Zou W. Chemokines in the cancer microenvironment and their relevance in cancer immunotherapy. *Nat Rev Immunol* 2017;17:559–72.
39 Steffen A, Ladwein M, Dimchev GA, *et al*. Rac function is crucial for cell migration but is not required for spreading and focal adhesion formation. *J Cell Sci* 2013;126:4572–88.
40 McLoughlin RM, Jenkins BJ, Grail D, *et al*. Il-6 trans-signaling via STAT3 directs T cell infiltration in acute inflammation. *Proc Natl Acad Sci U S A* 2005;102:9589–94.
41 Cacalano NA. Regulation of natural killer cell function by STAT3. *Front Immunol* 2016;7:128.
42 Hoogstad-van Evert JS, Maas RJ, van der Meer J, *et al*. Peritoneal NK cells are responsive to IL-15 and percentages are correlated with outcome in advanced ovarian cancer patients. *Oncotarget* 2018;9:34810–20.
43 Hoogstad-van Evert JS, Bekkers R, Ottevanger N, *et al*. Harnessing natural killer cells for the treatment of ovarian cancer. *Gynecol Oncol* 2020;157:810–6.
44 Varga A, Piha-Paul S, Ott PA, *et al*. Pembrolizumab in patients with programmed death ligand 1-positive advanced ovarian cancer: analysis of KEYNOTE-028. *Gynecol Oncol* 2019;152:243–50.
45 Mouw KW, Goldberg MS, Konstantinopoulos PA, *et al*. DNA damage and repair biomarkers of immunotherapy response. *Cancer Discov* 2017;7:675–93.
46 Chabanon RM, Rouanne M, Lord CJ, *et al*. Targeting the DNA damage response in immuno-oncology: developments and opportunities. *Nat Rev Cancer* 2021;21:701–17.
47 Zheng X-F, Acharya SS, Choe KN, *et al*. A mitotic CDK5-PP4 phospho-signaling cascade primes 53BP1 for DNA repair in G1. *Nat Commun* 2019;10:4252.
48 Wang B, Zhao A, Sun L, *et al*. Protein phosphatase PP4 is overexpressed in human breast and lung tumors. *Cell Res* 2008;18:974–7.
49 Leopold WR, Shillis JL, Mertus AE, *et al*. Anticancer activity of the structurally novel antibiotic CI-920 and its analogues. *Cancer Res* 1984;44:1928–34.
50 Lewy DS, Gauss C-M, Soenen DR, *et al*. Fostriecin: chemistry and biology. *Curr Med Chem* 2002;9:2005–32.
51 Theobald B, Bonness K, Musiyenko A, *et al*. Suppression of Ser/Thr phosphatase 4 (PP4C/*PPP4C*) mimics a novel post-mitotic action of fostriecin, producing mitotic slippage followed by tetraploid cell death. *Mol Cancer Res* 2013;11:845–55.
52 Böckelman C, Lassus H, Hemmes A, *et al*. Prognostic role of CIP2A expression in serous ovarian cancer. *Br J Cancer* 2011;105:989–95.

53 Le LH, Erlichman C, Pillon L, *et al*. Phase I and pharmacokinetic study of fostriecin given as an intravenous bolus daily for five consecutive days. *Invest New Drugs* 2004;22:159–67.
54 Swingle MR, Amable L, Lawhorn BG, *et al*. Structure-activity relationship studies of fostriecin, cytostatin, and key analogs, with PP1, PP2A, PP5, and (beta12-beta13)-chimeras (PP1/PP2A and PP5/PP2A), provide further insight into the inhibitory actions of fostriecin family inhibitors. *J Pharmacol Exp Ther* 2009;331:45–53.
55 McConnell JL, Wadzinski BE. Targeting protein serine/threonine phosphatases for drug development. *Mol Pharmacol* 2009;75:1249–61.
56 Mackenzie KJ, Carroll P, Martin C-A, *et al*. cGAS surveillance of micronuclei links genome instability to innate immunity. *Nature* 2017;548:461–5.
57 Ablasser A, Goldeck M, Cavlar T, *et al*. cGAS produces a 2'-5'-linked cyclic dinucleotide second messenger that activates sting. *Nature* 2013;498:380–4.
58 Woo S-R, Fuertes MB, Corrales L, *et al*. Sting-Dependent cytosolic DNA sensing mediates innate immune recognition of immunogenic tumors. *Immunity* 2014;41:830–42.
59 Sen T, Rodriguez BL, Chen L, *et al*. Targeting DNA damage response promotes antitumor immunity through STING-mediated T-cell activation in small cell lung cancer. *Cancer Discov* 2019;9:646–61.
60 Liang Y-K, Deng Z-K-, Chen M-T, *et al*. Cxcl9 is a potential biomarker of immune infiltration associated with favorable prognosis in ER-negative breast cancer. *Front Oncol* 2021;11:710286.
61 Seitz S, Dreyer TF, Stange C, *et al*. CXCL9 inhibits tumour growth and drives anti-PD-L1 therapy in ovarian cancer. *Br J Cancer* 2022;126:1470–80.
62 Reschke R, Yu J, Flood BA, *et al*. Immune cell and tumor cell-derived CXCL10 is indicative of immunotherapy response in metastatic melanoma. *J Immunother Cancer* 2021;9:e003521.
63 Saul D, Kosinsky RL, Atkinson EJ, *et al*. A new gene set identifies senescent cells and predicts senescence-associated pathways across tissues. *Nat Commun* 2022;13:4827.
64 Freund A, Patil CK, Campisi J. p38MAPK is a novel DNA damage response-independent regulator of the senescence-associated secretory phenotype. *Embo J* 2011;30:1536–48.
65 Glück S, Guey B, Gulen MF, *et al*. Innate immune sensing of cytosolic chromatin fragments through cGAS promotes senescence. *Nat Cell Biol* 2017;19:1061–70.
66 Cohen PTW, Philp A, Vázquez-Martin C. Protein phosphatase 4--from obscurity to vital functions. *FEBS Lett* 2005;579:3278–86.
67 Prager I, Watzl C. Mechanisms of natural killer cell-mediated cellular cytotoxicity. *J Leukoc Biol* 2019;105:1319–29.
68 Fauriat C, Long EO, Ljunggren H-G, *et al*. Regulation of human NK-cell cytokine and chemokine production by target cell recognition. *Blood* 2010;115:2167–76.
69 Henriksen JR, Donskov F, Waldstrøm M, *et al*. Favorable prognostic impact of natural killer cells and T cells in high-grade serous ovarian carcinoma. *Acta Oncol* 2020;59): :652–9.
70 Henriksen JR, Nederby L, Donskov F, *et al*. Blood natural killer cells during treatment in recurrent ovarian cancer. *Acta Oncol* 2020;59:1365–73.
71 Muntasell A, Rojo F, Servitja S, *et al*. NK cell infiltrates and HLA class I expression in primary HER2$^+$ breast cancer predict and uncouple pathological response and disease-free survival. *Clin Cancer Res* 2019;25:1535–45.
72 Ali TH, Pisanti S, Ciaglia E, *et al*. Enrichment of CD56(dim)KIR + CD57 + highly cytotoxic NK cells in tumour-infiltrated lymph nodes of melanoma patients. *Nat Commun* 2014;5:5639.

Supplementary Figure 1: Genetic alterations of PP4 complex in ovarian cancer. (A) Oncoprint showing genetic and transcript level alterations of PP4 in ovarian cancer (n=202). The image was generated using cBioportal. (B) Comparison of RNA expression versus copy number for *PPP4R3A*, *PPP4R3B* and *PPP4R2* from pan-cancer TCGA data is plotted as bar graph, ****p<0.0001. (C) The transcript level expression of PPP4C along with proteomics score was obtained from Depmap portal and plotted as graph with RNA level expression on left -Y axis and proteomics score on right -Y axis. Proteomics score for PP4C was not available for OVCAR5 and 59M.

Supplementary Figure 1

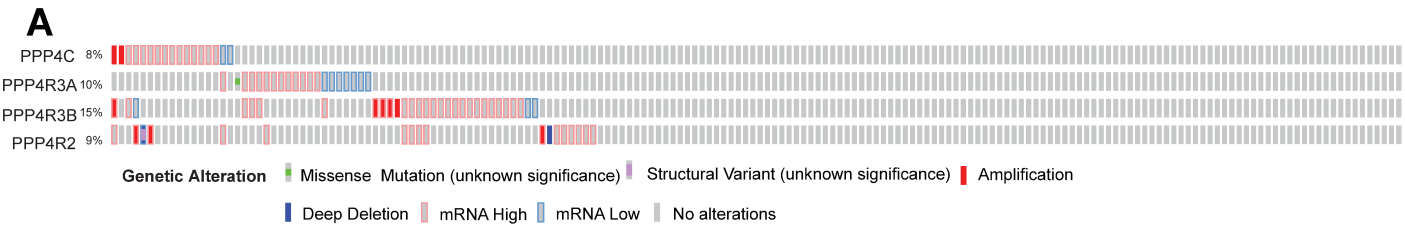

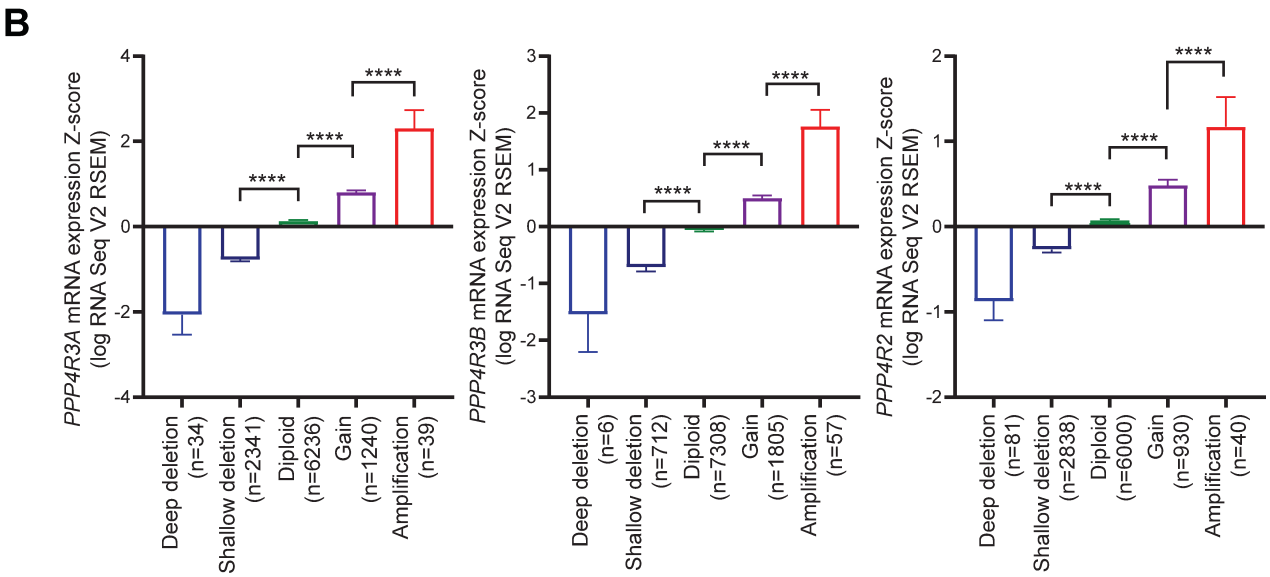

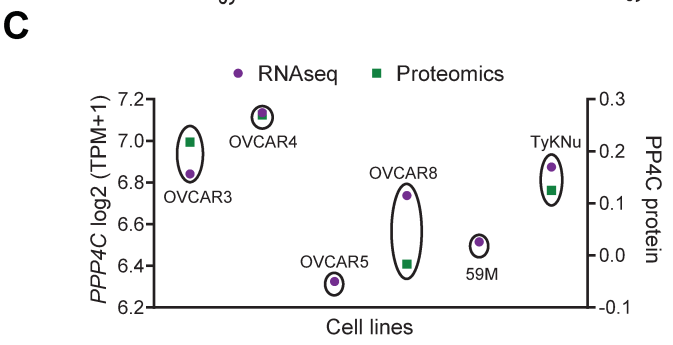

Supplementary Figure 2: Generation and p53 CRISPR knockout validation in ID8 mouse ovarian cancer cells. (A) Sequence of the target region of *TP53* gene from reference genome (black) non-targeting control, NTC (blue), and Trp53-/- clone E12e (green) are shown (top panel). gRNA sequences used to generate the clone are underlined. Sanger sequencing of the region around exon 5 of *TP53*-/- clone E12e and NTC are shown. The deleted region is highlighted in red and break points indicated in clone E12e (bottom panel). (B) Representative PCR of 538 base pair region spanning the targeted exon 5, showing deletion in ID8 E12e clone compared to NTC control. (C) Expression of p53 was determined in parental ID8 and three *TP53*-/- clones± carboplatin (100 µM) by immunoblot. Actin was used as loading control.

Supplementary Figure 2

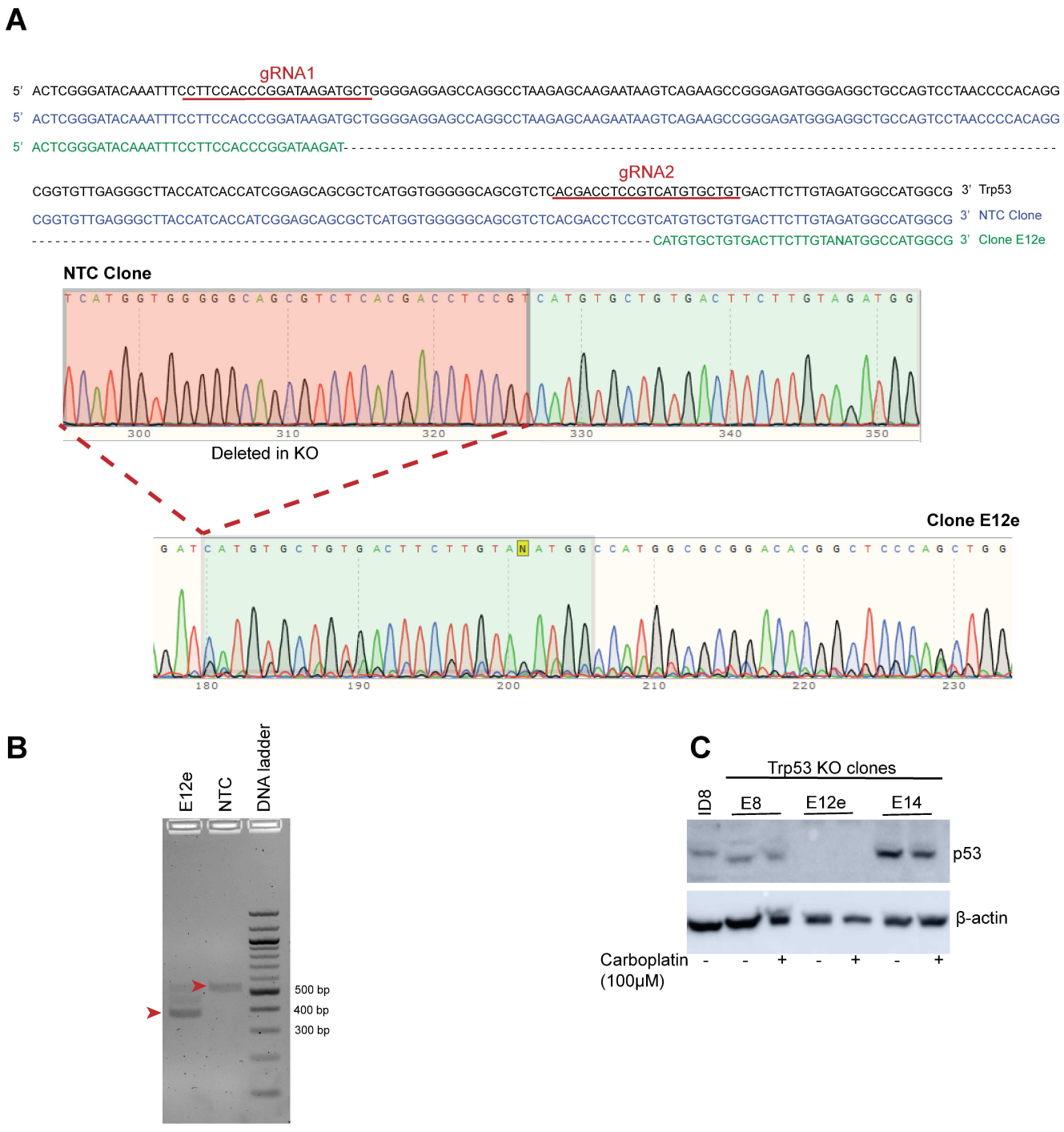

Supplementary Figure 3: Workflow for determining PP4 phosphatase activity is shown. Immunopurified PP4 complex in OVCAR3 and OVCAR4 cells were incubated with Fos (1nM) for 30 min. After substrate addition, relative fluorescence was measured and quantified. The results represented here are the average of 3 independent experiments $\pm$SEM, *$p < 0.05$.

Supplementary Figure 3

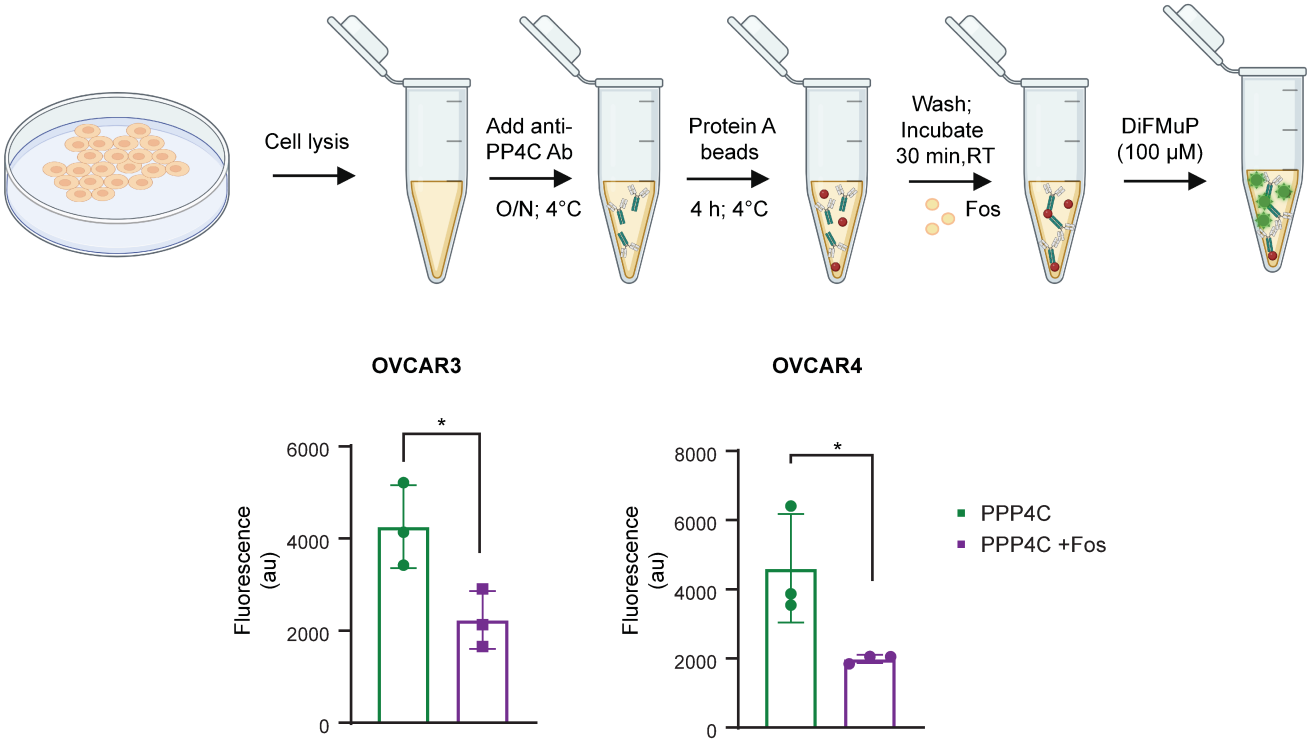

Supplementary Figure 4: Fostriecin augments carboplatin-induced DNA damage in OC cell lines. (A) Representative images of micronuclei formed upon 24 h fostriecin pre-treatment ± carboplatin treatment in ovarian cancer cell lines. (B). Immunoblot analysis showing relative changes in γ-H2AX (S139) in OC cell lines treated ± Fos (1nM) and carboplatin treatment at 96 h. Corresponding total H2AX and actin are also shown. (C) Quantification of FANCD2 and γ-H2AX (S139) staining intensities (derived from the high throughput image analysis) were compared across different treatment groups. An average from 70-90 sites is represented as violin plots, $p<0.0001$.

Supplementary Figure 4

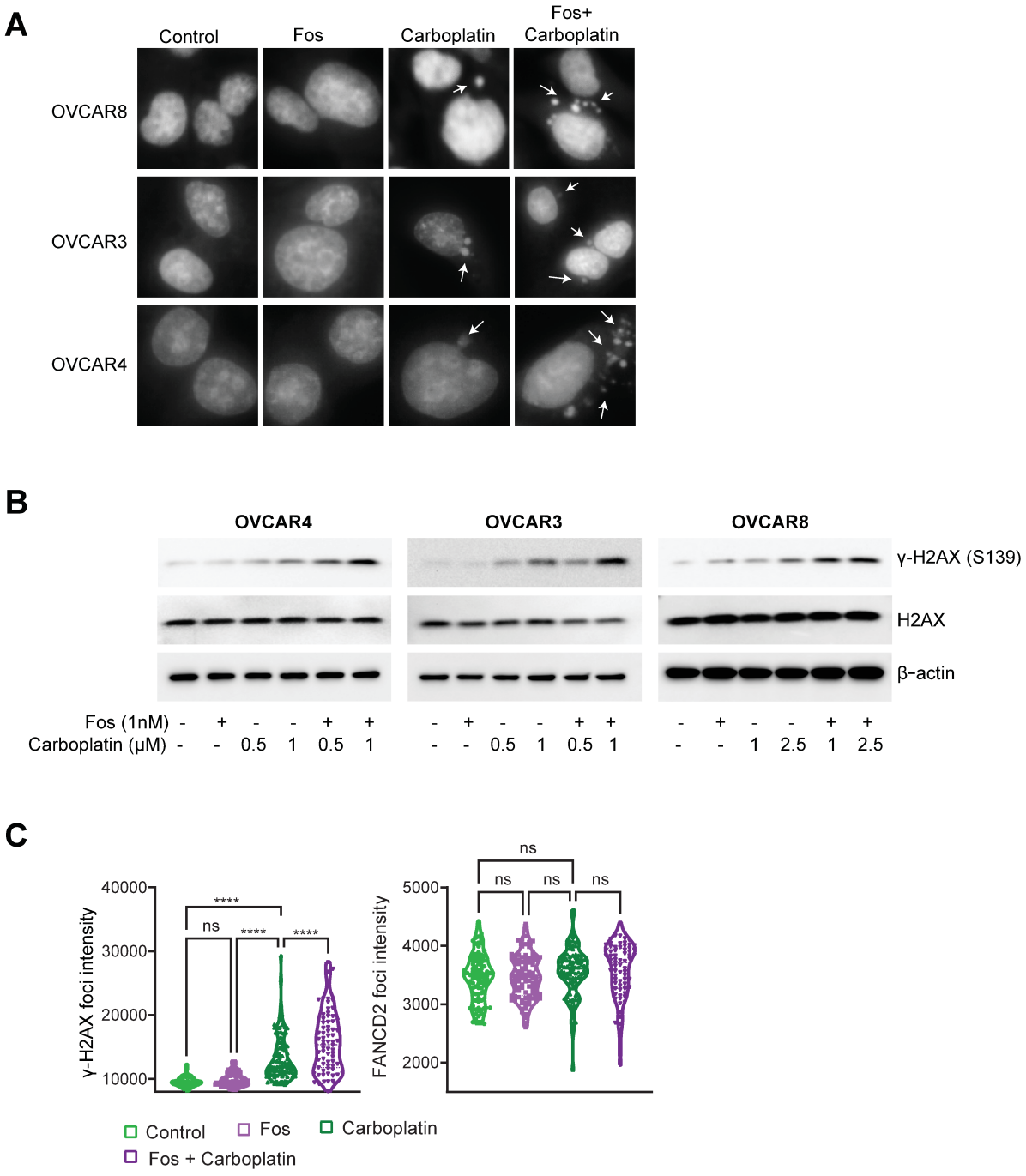

Supplementary Figure 5: Loss of PP4 leads to increased inflammatory signaling and cytokine production in ID8-p53KO cells. (A) ID8-p53KO cells were pre-treated ± Fos (1nM) for 24 h, followed by carboplatin (10μM). On day 5, cells were harvested and immunoblot analysis was performed to determine STAT1 phosphorylation levels across treatment groups. (B) ID8-p53KO cells were transfected with *PPP4C* siRNA followed by carboplatin (10μM). STAT1 phosphorylation is shown by western blot. (C) i, ii Quantitative PCR for *CCL5, CXCL10, IL6* and *IFNB1* in human OVCAR3 and OVCAR8 cells following 24 h Fos pre-treatment ± carboplatin treatment. Mean±SEM, *p<0.05, **p<0.01, ****p<0.0001. (D&E) Transcript levels of *CCL5*, *CXCL10*, *IL6* and *IFNB1* following either Fos treatment or *PPP4C* siRNA transfection ± carboplatin in ID8-p53KO were measured by quantitative PCR and the relative fold change was calculated from 3 replicates represented as a bar graph. *p<0.05, * *p<0.01, ***p<0.001 and****p<0.0001.

Supplementary Figure 5

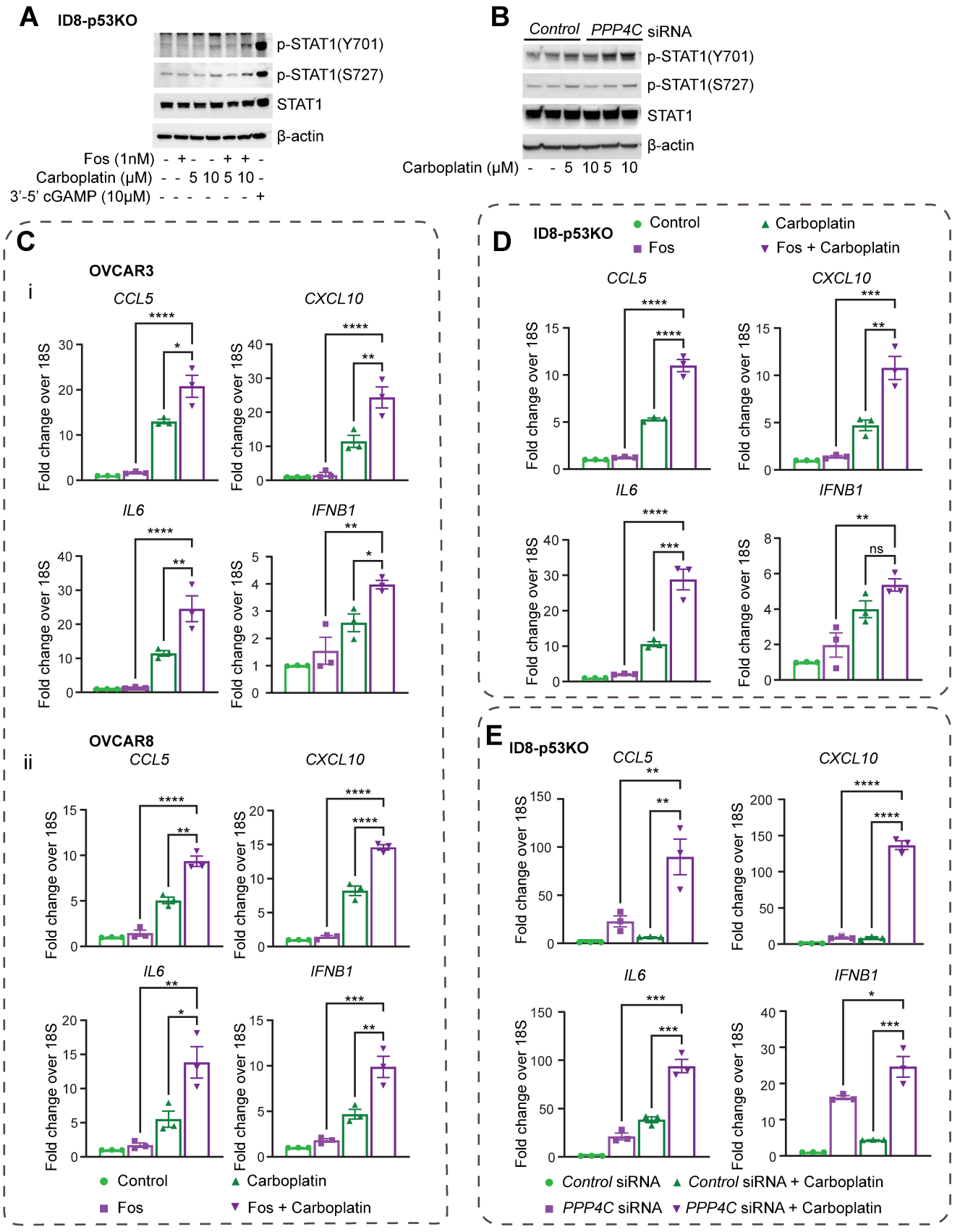

Supplementary Figure 6: (A) Direct fostriecin treatment does not affect CD8 T cell activation**.** Splenocytes were harvested from OT I mice and stimulated with OVA peptide (SIINFEKL) in the presence of varying doses of fostriecin. On Day 4, cells were restimulated with OVA in the presence of fostriecin and stained for intracellular TNFα and IFNγ. Representative flow plots showing IFNγ and TNFα expression in OT-I splenocytes are shown. The percentage of cells expressing TNFα and IFNγ across treatment conditions is represented as bar graph (n=3). (B) Immunoblot showing STING1 protein levels in OVCAR8 cells transfected with either control or *STING1* siRNA and treated with Fos and carboplatin. Actin was used as loading control.

Supplementary Figure 6

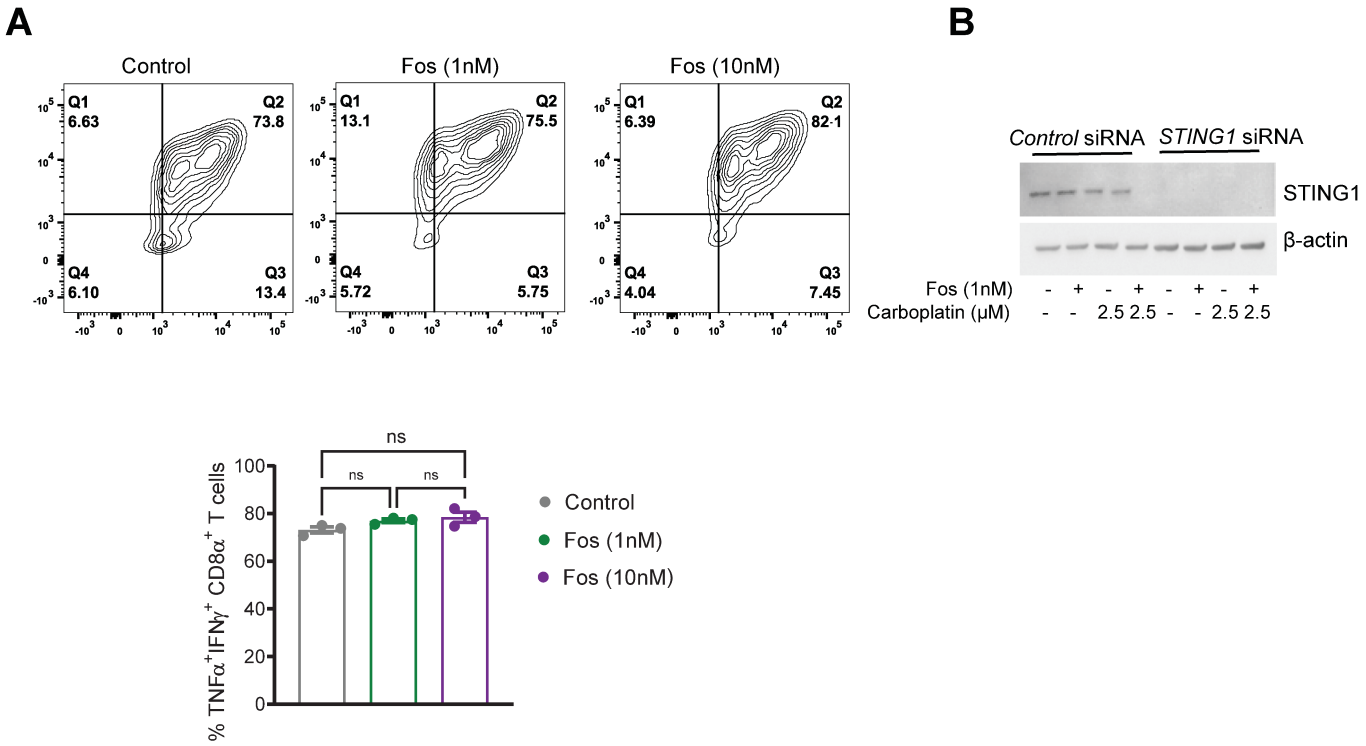

Supplementary Figure 7: PP4 subunit expression and immune cell infiltration. Correlation between the expression of PP4 subunits and infiltrating level of NK cells and NKT in ovarian cancer using CIBERSORT and xCELL on TIMER2.0 platform. Partial Rho and p values along with purity correction are shown.

Supplementary Figure 7

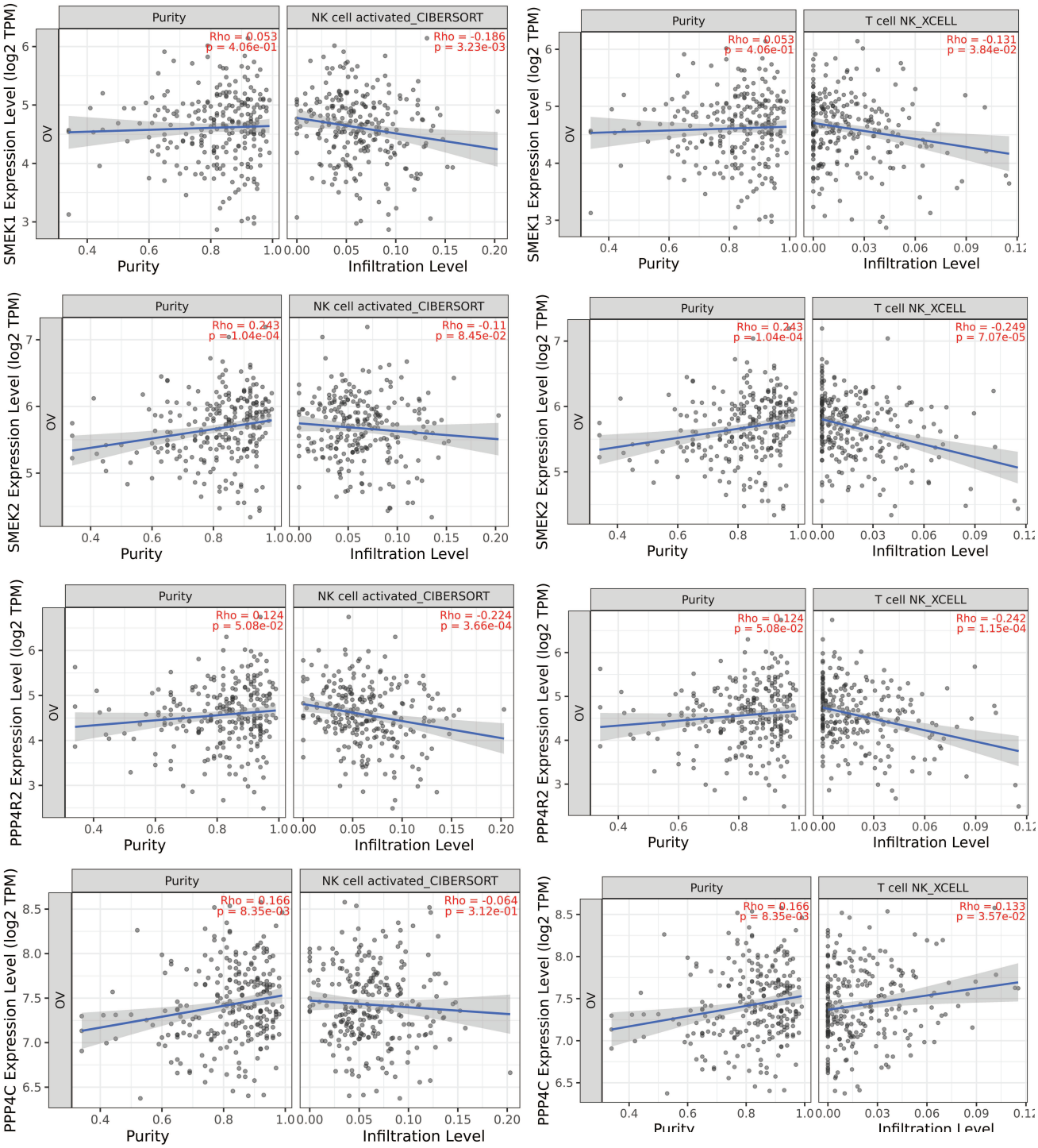

Supplementary Figure 8: NK cell-mediated killing of OC cells. (A) OVCAR3 cells were transfected with control*, PPP4C*, or *PPP4R3B* siRNA and treated ± carboplatin (2.5μM). Following co-culture with NK-92 cells, the OC cells were stained with Annexin V and PI and the CD45-negative cells were analyzed. Percentage of early and total apoptotic cells are shown for all treatment groups (n=4), ± SD, *p<0.05 and **p<0.01. (B) Representative flow plots showing Annexin V and PI positive cells following *control*, *PPP4C*, or *PPP4R3B* siRNA transfection are shown in the absence of NK-92 cells. Percentage of early and late apoptotic cells are shown as bar graphs (n=3), mean±SEM, ns-not significant.

Supplementary Figure 8

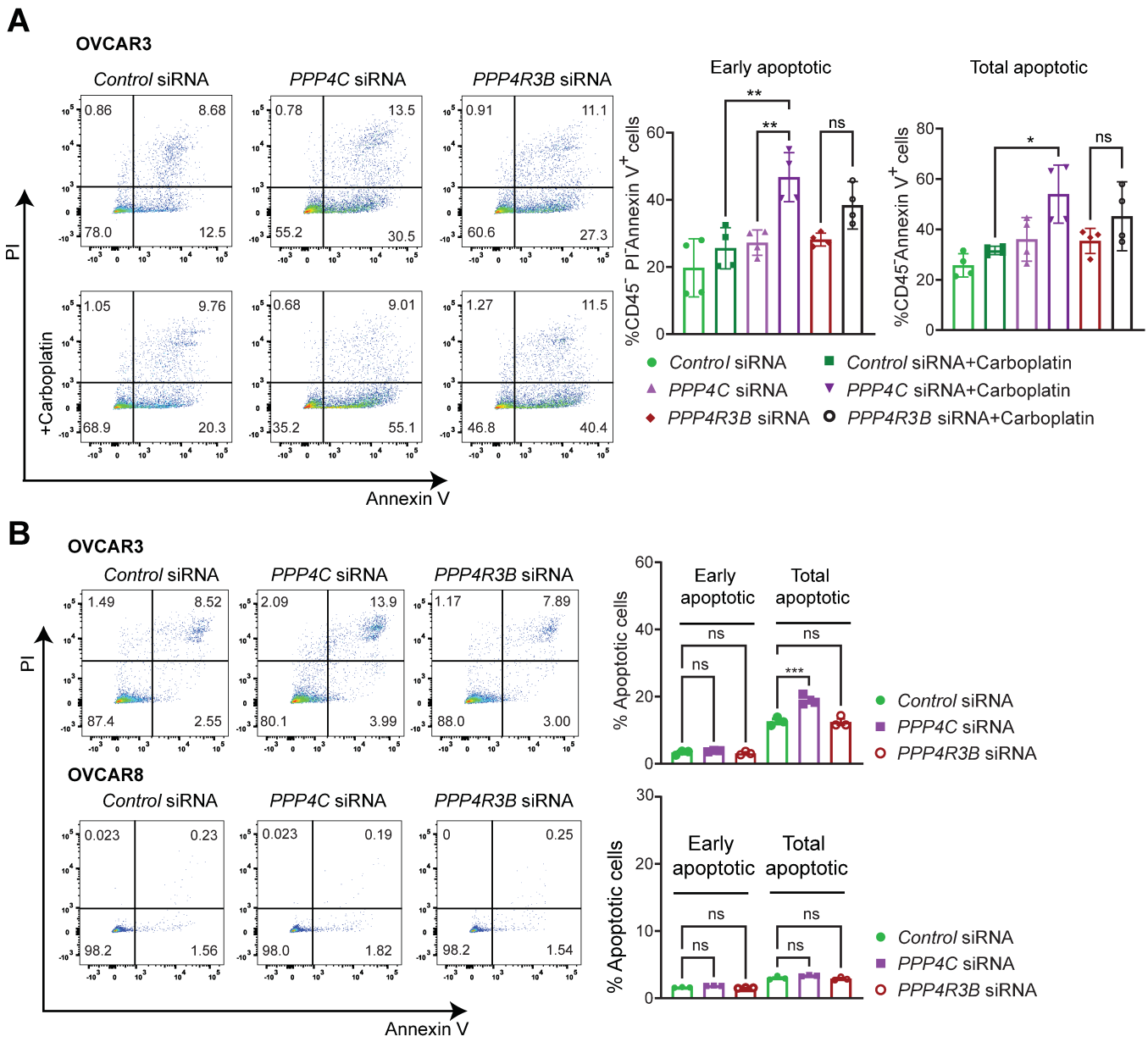

Supplementary Figure 9: Immune cell populations were identified by flow cytometry from spleen, peritoneal lymph nodes, and ascites. (A-C; i-iii) $CD3^{-}CD161^{+}$ and $CD3^{+}CD161^{+}$ cells per 10^3 live cells from spleen, peritoneal lymph nodes, and ascites, mean±SEM, ns-not significant. (D) Quantitation of IFNγ in $CD3^{-}CD161^{+}$ NK cells following *ex vivo* restimulation with PMA/ionomycin for 4 h, mean±SEM, ns-not significant. (E, F) $CD8^{+}$ and $CD4^{+}$ T cells per 10^3 live cells, mean±SEM, *p<0.05, **p<0.01. (G) $CD4^{+}CD25^{+}$ T cell population per 10^3 live cells from spleen, mesenteric lymph nodes and ascites, mean±SEM, *p<0.05.

Supplementary Figure 9

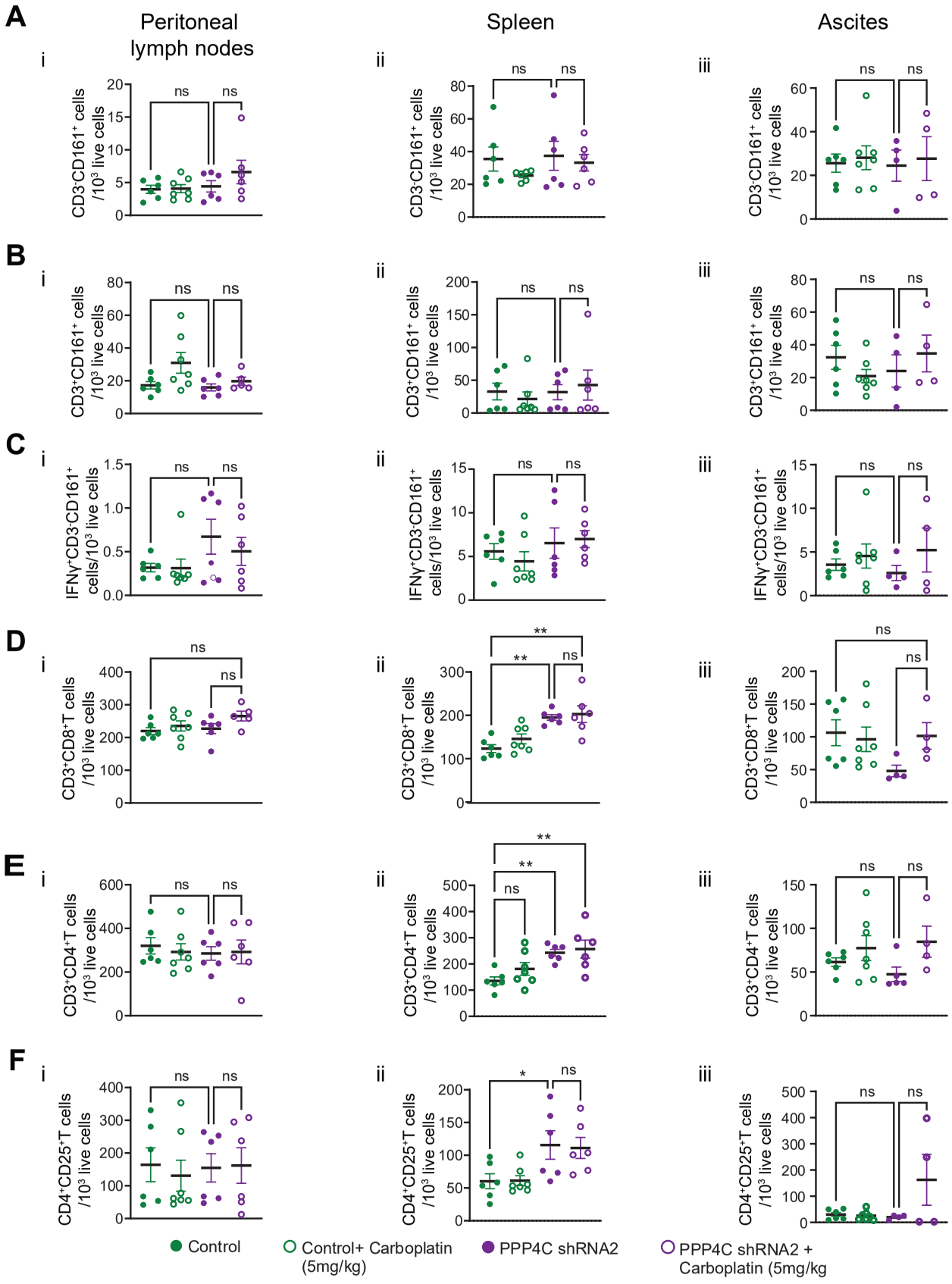

Raja R, *et al. J Immunother Cancer* 2022; 10:e005026. doi: 10.1136/jitc-2022-005026

Supplementary Figure 10: Immunophenotyping gating strategy. A representative sample is shown.

Supplementary Figure 10

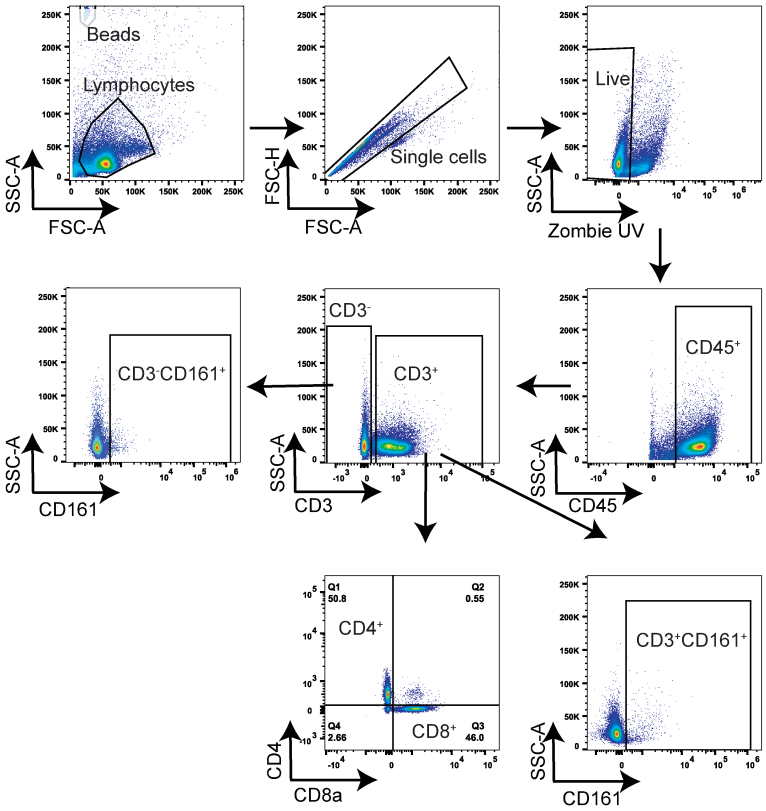

Supplementary Tables: -

Supplementary Table 1. CRISPR crRNA sequences used in the study for mouse

Gene	Catalog number (IDT)	Sequence
Trp 53	Mm.Cas9.TRP53.1.AG	GAAGTCACAGCACATGACGG (Same sequence as Guide R used in Walton *et al* Cancer Res. 2016)
	Mm.Cas9.TRP53.1. AB	GCGCTGACCCACAACTGCAC
	Mm.Cas9.TRP53.1. AA	CTTCCACCCGGATAAGATGC

Supplementary Table 2. List of antibodies used for immunoblotting and inhibitors used in the study

Antibody	Company	Catalog Number
PPP4C	Bethyl Laboratories	A300-835A-M
PPP4R3B	Bethyl Laboratories	A300-842A-M
PPP4R3A	Thermo Fischer Scientific	PA5-97089
PPP4R2	Bethyl Laboratories	A300-838A
P53	Santa Cruz Biotechnology	sc-126
Phospho-Histone H2AX	Cell Signaling	9718S
p-STAT1 (Y701)	Cell Signaling	9167S
p-STAT1 (S727)	Cell Signaling	9177S
STAT1 (D1K9Y)	Cell Signaling	14994T
Phospho-p65 (S536)	Cell Signaling	3033T
P65	Cell Signaling	6956T
STING	Cell Signaling	38866T
Fostiecin	Tochris Biosciences	#1840
STATTIC	Medchem Express	HY-13818
Trametinib	Medchem Express	HY-10999
NSC23766	Sigma Aldrich	SML0952

Supplementary Table 3. List of Taqman probes used in the study

Gene symbol	Company	Catalog Number: 4331182 Assay Number
CXCL10 (human)	Thermo Fisher Scientific	Hs00171042_m1
CXCL10 (mouse)	Thermo Fisher Scientific	Mm00445235_m1
IL6 (human)	Thermo Fisher Scientific	Hs00174131_m1
IL6 (mouse)	Thermo Fisher Scientific	Mm00446190_m1
IFNB1 (human)	Thermo Fisher Scientific	Hs01077958_s1
IFNB1 (mouse)	Thermo Fisher Scientific	Mm00439552_s1
CCL5 (human)	Thermo Fisher Scientific	Hs00982282_m1
CCL5 (mouse)	Thermo Fisher Scientific	Mm01302427_m1
18srRNA (human)	Thermo Fisher Scientific	Hs99999901_s1
18srRNA (mouse)	Thermo Fisher Scientific	Mm04277571_s1

Supplementary Table 4. List of antibodies used for flow cytometry in the study

Antibody	Company	Catalog Number
Ghost Dye UV 450	Tonbo Biosciences	13-0868-T500
CD3 (anti-mouse)	Tonbo Biosciences	70-0032-U500
CD8a (anti-mouse)	Tonbo Biosciences	75-0081-U100
TNFA (anti-mouse)	BioLegend	506308
IFNG (anti-mouse)	Tonbo Biosciences	50-7311-U100
CD45 (anti-human)	Tonbo Biosciences	25-0459-T100
TNFA (anti-human)	BioLegend	502932
IFNG (anti-human)	BioLegend	502509
CD107a (anti-human)	BioLegend	328640
Annexin V	BD Biosciences	556419
CD45 (anti-mouse)	BioLegend	103155
CD25 (anti-mouse)	BioLegend	102010
CD161 (NK1.1)	BioLegend	108730
PD1 (anti-mouse	BioLegend	135208
LAG3 (anti-mouse)	BioLegend	125243
Granzyme B (anti-mouse)	BioLegend	372204

Supplementary Table 5. List of genetic alterations in the cell lines used in the study

	BRCA1	BRCA2	TP53	KRAS	CCNE	ERBB2	PTEN	RB1	MYC
OVCAR3	WT/LOH	WT/LOH	R248Q/LOH	GAIN	AMP	WT/LOH	WT	WT/LOH	GAIN
OVCAR4	WT/LOH	p.P2505L /LOH	p.L130V/LOH	WT	GAIN	WT/LOH	GAIN	LOH	GAIN
OVCAR5	WT	WT	WT	pG12V	WT	WT	WT	WT	
OVCAR8	WT/ Methylated	WT	Splice site mutation	p.P121H	GAIN	p.G776V	WT	WT	GAIN
TYK-nu	WT	WT	R175H	WT/LOH	WT	WT	WT	WT	GAIN
59M	WT	WT	p. HLIRVE193fs	GAIN	WT	WT	WT	GAIN	AMP
ID8	WT	WT	WT	WT	WT	WT	WT	WT	WT

WT- Wild Type; AMP-High level amplification; GAIN-Moderate copy number; LOH-Heterozygous deletion; Protein changes associated with missense mutations are provided.

Information on cell line mutations, copy number alterations and methylation was obtained from DepMap portal and other cell line characterization studies[1-3].

References:

1. Walton, J., et al., *CRISPR/Cas9-Mediated Trp53 and Brca2 Knockout to Generate Improved Murine Models of Ovarian High-Grade Serous Carcinoma.* Cancer Res, 2016. **76**(20): p. 6118-6129.
2. Domcke, S., et al., *Evaluating cell lines as tumour models by comparison of genomic profiles.* Nat Commun, 2013. **4**: p. 2126.
3. Stordal, B., et al., *BRCA1/2 mutation analysis in 41 ovarian cell lines reveals only one functionally deleterious BRCA1 mutation.* Mol Oncol, 2013. **7**(3): p. 567-79.